Recent Developments and Understanding of Novel Mixed Transition-Metal Oxides as Anodes in Lithium Ion Batteries

Yang Zhao, Xifei Li, Bo Yan, Dongbin Xiong, Dejun Li,* Stephen Lawes, and Xueliang Sun**

Mixed transition-metal oxides (MTMOs), including stannates, ferrites, cobaltates, and nickelates, have attracted increased attention in the application of high performance lithium-ion batteries. Compared with traditional metal oxides, MTMOs exhibit enormous potential as electrode materials in lithium-ion batteries originating from higher reversible capacity, better structural stability, and high electronic conductivity. Recent advancements in the rational design of novel MTMO micro/nanostructures for lithium-ion battery anodes are summarized and their energy storage mechanism is compared to transition-metal oxide anodes. In particular, the significant effects of the MTMO morphology, micro/nanostructure, and crystallinity on battery performance are highlighted. Furthermore, the future trends and prospects, as well as potential problems, are presented to further develop advanced MTMO anodes for more promising and large-scale commercial applications of lithium-ion batteries.

1. Introduction

The global energy shortage has led to increasing demand for highly efficient green energy, such as solar and wind power, as well as advanced energy storage devices to harness this energy. Lithium-ion batteries (LIBs) have become the most widely used energy storage systems for portable electronic devices such as laptops, mobile phones, medical microelectronic devices, and electrical vehicles due to their many outstanding features, including high energy density, no memory effect, low maintenance, and little self-discharge.[1–8] However, the growing requirements for better LIBs requires constant innovation, in terms of improved safety, longer lifetime, smaller size, lighter weight, and lower cost.[5,9,10] For these expectations, the key to improved LIB performance is in the electrode materials.[11] Presently, commercial anode materials mainly include graphite, which limits the lithium storage performance in terms of energy and power density due to the low theoretical capacity (LiC_6, 372 mAh g^{-1}) and low Li-ion transport rate.[12–14] New anode materials with higher capacities are being looked for including mixed transition metal oxide anodes.

1.1. Traditional Metal Oxide Anodes

New research is constantly being carried out to reach the high requirements for LIB anodes. Various metal oxide materials such as SnO_2,[15–19] Co_3O_4,[20–23] NiO,[24–27] Fe_3O_4,[28–30] and MnO_2[31–33] are alternative potential anodes for LIBs due to their high theoretical capacities, high power density, and wide usefulness. However, metal oxides inevitably suffer from several major problems: severe volume changes during the alloying-dealloying processes, pulverization and agglomeration of primitive particles, and poor electronic conductivity that hinders the reaction with lithium during electrochemical reactions. Numerous approaches have attempted to address these challenges. One useful method is to develop the metal oxide materials into nanostructures.[3] The distinct lithium storage mechanisms and the influence of unique structures on the lithium storage properties of the metal oxide materials have been reported in detail.[5] A series of work on the design of various nanostructures of metal oxide materials has been subsequently carried out, for nanomaterials of different dimensions, hollow structures, and hierarchical structures.[5] Coating or combining the buffering matrix or conductive materials with metal oxide materials is another way to relieve the severe problems.[36–42] Various carbon materials, especially novel nanocarbon materials like carbon nanotubes and graphene nanosheets, have been widely studied as the buffering and conductive agent for metal oxide anodes.[43–46] In our previous review,[47] the significant effects of graphene nanosheets on tin-based anodes were summarized in detail. It has been concluded that graphene not only contributes as a highly conductive network, but also as a flexible supporting layer, effectively relieving the volume change and particle aggregation. In addition, different metals and metal oxides that are electrochemically active and

Prof. X. Li, Y. Zhao, B. Yan, D. Xiong,
Prof. D. Li, Prof. X. L. Sun
Energy & Materials Engineering Center
College of Physics and Materials Science
Tianjin Normal University
Tianjin 300387, China
E-mail: xfli2011@hotmail.com; dejunli@mail.tjnu.edu.cn; xsun@eng.uwo.ca
Y. Zhao, S. Lawes, Prof. X. L. Sun
Nanomaterials and Energy Lab
Department of Mechanical and Materials Engineering
University of Western Ontario
London, Ontario N6A 5B9, Canada

DOI: 10.1002/aenm.201502175

exhibit low volume change have been introduced to combine with transition metals or transition metal oxides.[38,45,48,49] It is considered that the primary benefit of the additional materials is to provide a mechanical buffer for accommodating volume changes that otherwise would lead to disintegration.[50] However, traditional metal oxides cannot meet the requirements for application in LIBs, which still suffer from the problems of volume expansion and low conductivity. Based on these challenges, the mixed transition-metal oxides (MTMOs) attract more and more attention and show their great potential as anodes for LIBs.

1.2. Mixed Transition Metal Oxide Anodes

MTMOs, including stannates, ferrites, cobaltates and nickelates, refer to ternary metal oxides with two different metal cations, rather than mixtures of two binary metal oxides.[51] These kinds of metal-composite oxides have been used in various fields,[52] such as microwave absorption,[53–57] catalysts, supercapacitors,[58–61] dye-sensitized solar cells,[62–64] metal air batteries,[65–68] and especially LIBs.[69,70]

Compared with traditional metal oxides, MTMOs are attracting great research interest as anodes in LIBs owing to their remarkable features:

1) In MTMOs, the two types of metal elements have different expansion coefficients, which results in a synergistic effect. For example, with stannates there is an extra M_xO generated from the reaction of MTMOs with lithium, which acts as a soft matrix to buffer the volume expansion of Li alloying/de-alloying. A schematic representation of the main electrochemical processes of MTMOs can be seen in **Scheme 1**. 2) Generally, MTMOs can alloy with more Li ions compared to mixed and normal metal oxides,[71] owing to the complex chemical compositions and resulting in higher reversible capacities. Both elements in MTMOs are electrochemically active metals with respect to Li–metal, resulting in better electrochemical performance. 3) More significantly, these MTMOs usually exhibit higher electrical conductivity than simple metal oxides owing to the relatively low activation energy for electron transfer between cations. 4) MTMOs are often more environmental benign than the traditional metal oxides, particularly for cobalt oxides.[4]

As a result, much effort has been devoted to designing MTMOs and their composites as anode materials for LIBs, and a lot of work has been previously reported to discuss this hot topic. Unfortunately, few review papers were focused on summarizing MTMOs for the application of LIBs in detail, while MTMOs used in supercapacitors have been summarized in several feature articles,[225,226] Therefore, it is of importance to review the recent achievements and development of MTMOs as anodes for LIBs, which will accelerate further improvement and application of these types of anode materials. On the basis of this motivation, this review article focuses on different kinds of MTMOs as anodes for LIBs, particularly stannates and XM_2O_4 (M = Mo, Co, Fe, Mn) materials, including their Li-storage mechanisms, synthesis methods, reasonable structure design, and strategies for addressing the issues that have arisen.

Xifei Li is currently a full professor and Associate Dean of College of Physics and Materials Science at Tianjin Normal University. He obtained his Bachelor degree in electrochemistry at Harbin Institute of Technology in 2001, Master degree at General Research Institute for Nonferrous Metals in China in 2004, and PhD at Xi'an Jiaotong University in 2008. He then worked as a postdoctoral follow at Florida International University and University of Western Ontario. Since 2001 he has been focusing on various materials for energy storage and conversion. Dr. Li's research group is currently working on design, synthesis as well as performance improvement of the anodes and the cathodes with various structures for high performance lithium ion batteries, lithium sulfur batteries, sodium ion batteries, and supercapacitors.

Dejun Li is currently a full professor at Tianjin Normal University. He obtained his Bachelor degree in Physics at Tianjin Normal University in 1984, Ph.D degree in Solid State Physics at Tianjin Unversity in 1987, in Materials Physics and Chemistry at Tsinghua University in 1999. He then worked three years as a postdoctoral follow at Northwestern University of USA. Since 1999 he has been focusing on various thin films, coatings, and nanomaterials for protection, energy storage and conversion. His research group is currently working on design, synthesis, and applications of various coatings for surface modification of the electrodes of various high performance batteries and supercapacitors as well as tools.

Xueliang (Andy) Sun is a Senior Canada Research Chair (Tier 1) and Full Professor at the University of Western Ontario, Canada. Dr Sun received his PhD in Materials Chemistry under the direction of Prof. George Thompson in 1999 at the University of Manchester, UK, which he followed up by working as a postdoctoral fellow under the direction of Prof. Keith Mitchell at the University of British Columbia, Canada and as a Research Associate under the direction of Prof. Jean-Pol Dodelet at l'Institut national de la recherche scientifique (INRS), Canada. His current research interests are associated with advanced materials for electrochemical energy storage and conversion, including electrocatalysis and catalyst support in fuel cells and electrodes in lithium-ion batteries and metal–air batteries.

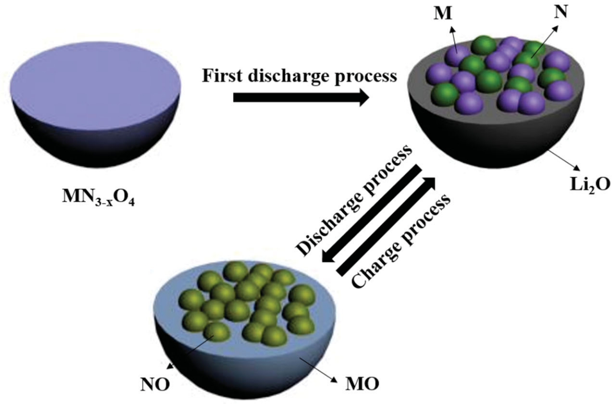

Scheme 1. Schematic representation of the main electrochemical processes of MTMOs.

2. Stannate Anodes

2.1. Li_2SnO_3 anodes

Li_2SnO_3 with the monoclinic crystal structure (**Figure 1**d) has been known to be a promising potential material for nuclear fusion reactors since their early stages.[74–77] As a Sn-based materials, it also shows great potential as an anode material for LIBs with the theoretical capacity of 1246 mAhg^{-1}.[78–80] In comparison to tin oxide, one extra inactive Li_2O is generated from the electrochemical reduction of Li_2SnO_3, which serves as a buffer to accommodate the volume change of the Li–Sn alloying/de-alloying reaction. The possible Li deintercalation/intercalation reaction, which can be expressed by:

$$Li_2SnO_3 + 4Li \rightarrow 3Li_2O + Sn$$

$$Sn + xLi \leftrightarrow LixSn\,(x \leq 4.4)$$

Studies show that the various synthesis methods of Li_2SnO_3 affect the obtained electrochemical properties. Normally, Li_2SnO_3 is synthesized in one of two ways[79]: via a solid-state reaction route (SSRR) or a sol–gel route. The morphology of Li_2SnO_3 prepared by these two methods can be seen in Figure 1a,b. The sol–gel derived Li_2SnO_3 is composed of uniform nano-sized particles (200–300 nm) and delivers a better reversible capacity (380 mAhg^{-1} after 50 cycles at a current of 60 mA g^{-1}) than that of the SSRR. Other approaches, such as a hydrothermal route,[81] have been employed to synthesize Li_2SnO_3. The obtained Li_2SnO_3 had a unique rodlike structure, displaying improved electrochemical performance and good cycling stability (510.2 mAhg^{-1} after 50 cycles at a current density of 60 mAg^{-1}, Figure 1e,f). It is believed that the smaller primary particle size of 50–60 nm (Figure 1c) and porous structure contribute to the performance improvements.

In a case of Li_2SnO_3 anode, although the extra Li_2O can be the buffering matrix for the large volume expansion of Sn, more Li_2O still results in the lower electronic conductivity. As a result, coating or combining Li_2SnO_3 with conducting material can be the useful way to address the problems, which not only can enhance the conductivity but also relief the volume changes causing great enhancement of the electrochemical properties of the anodes.[82] A series of studies have reported the effects of introducing different conductive systems, like carbon coatings,[83–85] conductive polymers,[86,87] and graphene,[88] into Li_2SnO_3. Their results demonstrate that the composites show better properties than the pristine phase. Two types of graphene

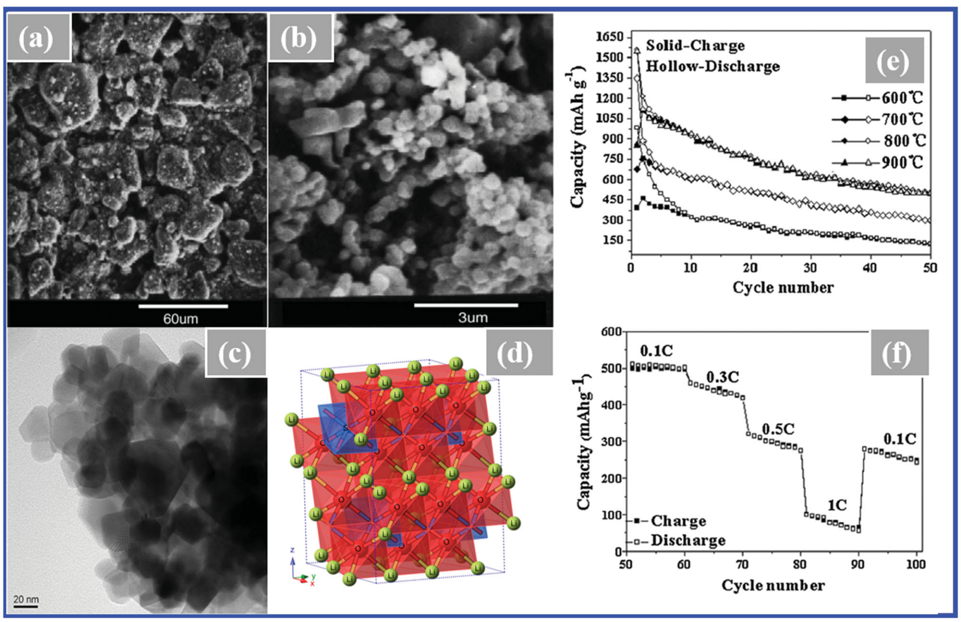

Figure 1. SEM images of Li_2SnO_3 particles synthesized by solid-state reaction route (a), and sol–gel route (b); Reproduced with permission.[79] Copyright 2006, Elsevier. c) TEM image of Li_2SnO_3 nanoparticles synthesized by hydrothermal route with the electrochemical performances of cycling (e), and rate (f) properties. Reproduced with permission.[81] Copyright 2013, Wiley. d) The crystal structure of monoclinic Li_2SnO_3.

ternary composites, C/Li_2SnO_3/graphene[89] and polypyrrole (PPy)/Li_2SnO_3/graphene,[90] were further designed to create double buffering matrices. A flexible and robust graphene support and an outer carbon or conductive polymer shell formed a novel sandwich structure that better confined the Li_2SnO_3 particles and improved the mechanical properties. Furthermore, Li_2SnO_3 nanoparticles encapsulated in the graphene and carbon (conductive polymer) matrix resulted in improved electrical conductivity, leading to improved cycling performance and higher capacities compared with the pristine and binary nanocomposites.

Actually, compared with other stannates, the advantages of Li_2SnO_3 are not obvious. The extra Li_2O will greatly decrease the conductivity of Li_2SnO_3. When the Sn nanoparticles become surrounded with Li_2O, electron and Li ion diffusion is significantly reduced, which negatively affects the performance. More electrochemically inactive Li_2O leads to more irreversible capacity and a lower initial Coulombic efficiency. However, one cannot neglect the beneficial function of Li_2O for Sn-based anode materials, as the serious volume change is still a big challenge. Thus, effective strategies for Li_2SnO_3 must design hierarchical nanostructures to shorten the distance of electron and lithium-ion transport, as well as improve the conductivity of Li_2SnO_3, which will allow Li_2O to have the greatest positive effect.

2.2. $CoSnO_3$ and Co_2SnO_4 Anodes

As one of the stannates, Co_xSnO_y (x = 1, 2; y = 3, 4) has also been realized as an anode material for LIBs.[91,92] In Co_xSnO_y, cobalt or cobalt oxide can take part in the oxidation and reduction processes, which would result in enhanced performance due to another active phase. However, Co_xSnO_y greatly differs from a simple mixture of SnO_2 and CoO, especially in the application of LIB anodes. Both the $CoSnO_3$ and Co_2SnO_4 generally show the cubic spinel crystal structure (crystal structure of Co_2SnO_4 is shown in **Figure 2**g) with the theoretical capacity of 1238 mA h g^{-1} and 1105 mA h g^{-1}, respectively. The electrochemical performance of $CoSnO_3$ and the mixture of SnO_2 and CoO have been compared[92] and it was found that $CoSnO_3$ shows much better performance due to the more homogeneous distribution of Co and Sn in the first discharge process.

In early studies, the conventional solid-state reaction route was always used for the production of cobalt stannates,[98] which resulted in poor cycling stability due to large particle sizes and a broad particle size distribution. Thus, the synthesis methods were optimized. For example, cubic spinel Co_2SnO_4 nanocrystals were successfully synthesized via a simple hydrothermal reaction.[93] In the SEM images of Figure 2a,b, the particles synthesized via a hydrothermal reaction are smaller and have a more uniform size distribution than those produced by SSRR, resulting in better capacity retention. However, due to severe electrode pulverization caused by large volume change during the oxidation and reduction processes, the capacity retention of 50.3% was not sufficient for LIB anode requirements. Thus, a novel hollow $CoSnO_3$ nanobox was designed,[99] where the unique hollow interior provides a highly flexible structure, large electrode-electrolyte interface, and reduced diffusion path.[99–101] The obtained hollow nanobox exhibits high capacities of 520–620 mAh g^{-1} with stable capacity retention of over 80–90% after 60 cycles. Moreover, carbon coating has been further attempted to modify the hollow boxes to improve the anode performance.[95] The TEM image of $CoSnO_3$@C nanoboxes in Figure 2d shows that the surface of the nanoboxes is completely covered with a continuous amorphous carbon layer with uniform thickness of around 10 nm.[95] The $CoSnO_3$@C nanoboxes exhibit an exceptional cycle life of over 400 cycles and improved rate capability, as shown in **Figure 3**c.

Various methods for synthesizing different carbon/cobalt stannates have been reported.[94,102,103] Hydrothermally derived Co_2SnO_4 particles encapsulated with carbon are confirmed in the TEM image of Figure 2c, with a carbon thickness of approximately 20 nm. The composites demonstrate excellent cycling stability with capacity retention of 81% after 20 cycles. In general, carbon coating is an effective method to improve the electrochemical performance of cobalt stannates.

As a novel carbon nanomaterial, graphene can also be used enhance the electrochemical performance of stannates. Cobalt stannate/graphene composites have been designed to study lithium storage performance. $CoSnO_3$/GNS nanohybrids (Figure 2f) and Co_2SnO_4HC@rGOcomposites (Figure 2e) were

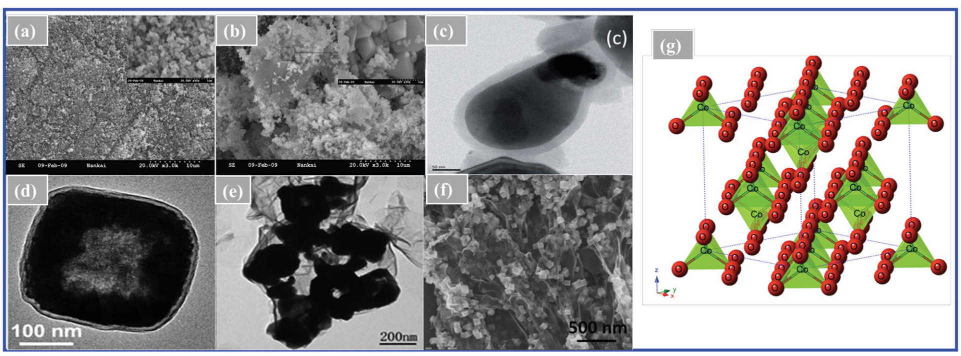

Figure 2. SEM images of Co_2SnO_4 particles synthesized by a) SSRR, and b) hydrothermal method. a,b) Reproduced with permission.[93] Copyright 2009, Elsevier. c) TEM image of Co_2SnO_4@C nanocomposites. Reproduced with permission.[94] Copyright 2014, Royal Society of Chemistry. d) TEM image of $CoSnO_3$@C nanoboxes. Reproduced with permission.[95] Copyright 2013, Royal Society of Chemistry. e) TEM image of Co_2SnO_4HC@rGOcomposites. Reproduced with permission.[96] Copyright 2014, Royal Society of Chemistry. f) SEM image of $CoSnO_3$/GNS nanohybrids. Reproduced with permission.[97] Copyright 2014, Elsevier. g) The crystal structure of cubic spinel Co_2SnO_4.

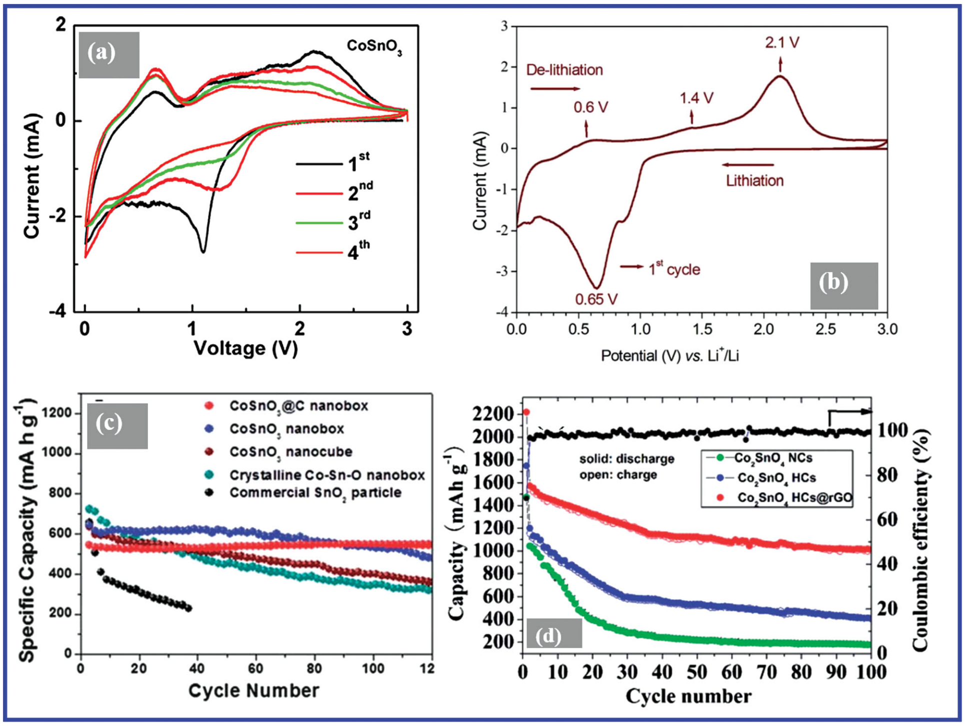

Figure 3. CV plots of $CoSnO_3$ (a) and Co_2SnO_4 (b) electrodes; Reproduced with permission.[94] Copyright 2014, Royal Society of Chemistry. Reproduced with permission.[97] Copyright 2014, Elsevier. c) Comparative cycling performance of $CoSnO_3$ nanoboxes with and without carbon coating, $CoSnO_3$ nanocubes, crystalline Co–Sn–O nanoboxes and commercial SnO_2 particles. Reproduced with permission.[95] Copyright 2013, Royal Society of Chemistry. d) Cycling performance of Co_2SnO_4HC@rGO composites and Co_2SnO_4 HC. Reproduced with permission.[96] Copyright 2014, Royal Society of Chemistry.

synthesized by thermal annealing and electrostatic interactions, respectively. The TEM images in Figure 2e and f show the structures of these two kinds of cobalt stannate/graphene composites.[96,97] Both of the composites exhibit excellent properties, retaining 649 mAh g^{-1} after 50 cycles and 1000 mAh g^{-1} over 100 cycles, respectively. The graphene coating improves the structural stability, the lithium storage kinetics, and the electron transport for both cobalt stannates. Thus, as shown in Figure 3d, the performance of Co_2SnO_4 HC@rGO composites is rapidly improved compared to Co_2SnO_4 HC. Recently, polystyrene spheres were used as sacrificial template for creating porous structure, and a novel type of $CoSnO_3$ nanoparticles encapsulated by porous graphene network was successfully created.[227] The designed $CoSnO_3$⊂porous graphene nanosheets show excellent electrochemical performances, including long cycle life and high rate capabilities, which originates from the improved electrical conductivity and stabilized SEI formation from graphene frameworks as well as the facilitation of Li-ions transport and accommodation of large volume expansion benefitting from interconnected nanosized pores.

In order to understand the electrochemical reaction mechanism of cobalt stannates, CV measurements were performed to investigate the electrode kinetics of $CoSnO_3$ and Co_2SnO_4, shown in Figure 3a and b, respectively.[94,97] Interestingly, it can be observed that $CoSnO_3$ has a higher initial reaction voltage platform (1.1 V) than that of Co_2SnO_4 (0.65 V), corresponding to the decomposition of cobalt stannate in the first discharge. However, the anodic peak locations are consistent for these two cobalt stannates and can be attributed to the de-alloying process (0.6 V), the re-oxidation reaction of tin (1.4 V) and the re-oxidation reaction of cobalt (2.1 V). As a result, the reaction of $CoSnO_3$ with Li can be expressed as:[97]

$$CoSnO_3 + 6Li^+ + 6e- \rightarrow Co + Sn + 3Li_2O$$

$$xLi^+ + Sn + xe^- \leftrightarrow Li_xSn\,(x \le 4.4)$$

$$Sn + 2Li_2O \leftrightarrow SnO_2 + 4Li^+ + 4e^-$$

$$Co + Li_2O \leftrightarrow 2Li^+ + 2e^- + CoO$$

Similar reactions of Co_2SnO_4 with Li can be written as:[94]

$$Co_2SnO_4 + 8Li^+ + e^- \rightarrow 2Co + Sn + 4Li_2O$$

$$xLi^+ + Sn + xe^- \leftrightarrow Li_xSn\,(x \le 4.4)$$

$$Sn + 2Li_2O \rightarrow SnO_2 + 4Li^+ + 4e$$

$$Co + Li_2O \leftrightarrow CoO + 2Li^+ + 2e^-$$

The CV results provide evidence for the electrochemical reaction mechanism. During the reaction of $CoSnO_3$ and Co_2SnO_4 with Li, Sn contributes most of the capacity for lithium storage. However, Co can further react with Li_2O produced in the first step of lithium insertion to provide extra capacity due to this conversion reaction.[97]

Based on the discussion above, cobalt stannates show great potential as anodes for LIBs. The mechanism of cobalt stannates is different from Li_2SnO_3. Metal cobalt is formed in the first step which can then react with Li_2O to contribute additional capacity. Additionally, the conductivity of metal cobalt is quite high, allowing it to act as a conductive matrix for the Sn particles due to the homogeneous formation of Co and Sn in the electrochemical process. However, the large volume change of Sn is still the main problem, which leads to capacity fading. Thus, finding an approach to improve the stability of cobalt stannates is a significant goal for researchers today.

2.3. $ZnSnO_3$ and Zn_2SnO_4 Anodes

Among all the stannates, zinc stannate is one of the most widely researched materials and has been applied in various fields, such as gas sensors,[104–108] solar cells,[109–112] photocatalysts,[113–115] and LIBs,[116,117] In the electrochemical processes of zinc stannates, multi-electron reactions are predominant, leading to a higher electrochemical capacity.[118] In principle, the theoretical capacity of $ZnSnO_3$ and Zn_2SnO_4 are 1317 and 1145 mA h g^{-1}, respectively. This is similar to cobalt stannates discussed above. The electrochemical reactions of $ZnSnO_3$ can be written as:

$$6Li^+ + ZnSnO_3 + 6e^- \leftrightarrow Zn + Sn + 3Li_2O$$

$$xLi^+ + Sn + xe^- \rightarrow Li_xSn(x \le 4.4)$$

$$yLi^+ + Zn + ye^- \leftrightarrow Li_yZn(y \le 1)$$

Analogous electrochemical reactions of Zn_2SnO_4 can be written as:

$$8Li^+ + Zn_2SnO_4 + 8e^- \rightarrow 2Zn + Sn + 4Li_2O$$

$$xLi^+ + Sn + xe^- \leftrightarrow Li_xSn(x \le 4.4)$$

$$yLi^+ + Zn + ye- \leftrightarrow Li_yZn(y \le 1)$$

The electrochemical behavior of Zn_2SnO_4 with lithium was investigated via XRD measurements.[119] The XRD analysis in **Figure 4**a verifies the aforementioned electrochemical reactions, which indicates the alloying and dealloying processes of Zn_2SnO_4 in the first charge–discharge reaction. In the first cathodic scan of the $ZnSnO_3$@C sample (see Figure 4b, the peak at 0.79 V is most probably due to the reduction of $ZnSnO_3$, whereas the sharp peaks at 0.6 and 0.4 V in Figure 4c correspond to the decomposition of Zn_2SnO_4 nanowires.[120,121] In the case of $ZnSnO_3$@C composites, the two peaks positioned at 0.32 and 0.13 V are related to the alloying of Sn and Zn with Li. The two peaks combine into one peak and are slightly shifted to ≈0.39 V in subsequent scans, indicating the formation of various Li_xSn and Li_yZn species. The anodic peak at 0.69 V is attributed to a de-alloying reaction of Li_xSn and Li_yZn to Sn and Zn, while the subsequent 1.27 V peak originates from the partially reversible oxidation of Sn and Zn.[120] The CV scans of Zn_2SnO_4 show almost the same peaks due to similar electrochemical reactions.

The hydrothermal method is one of the most common preparation routes for zinc stannate.[115,116,126,127] The inverse spinel

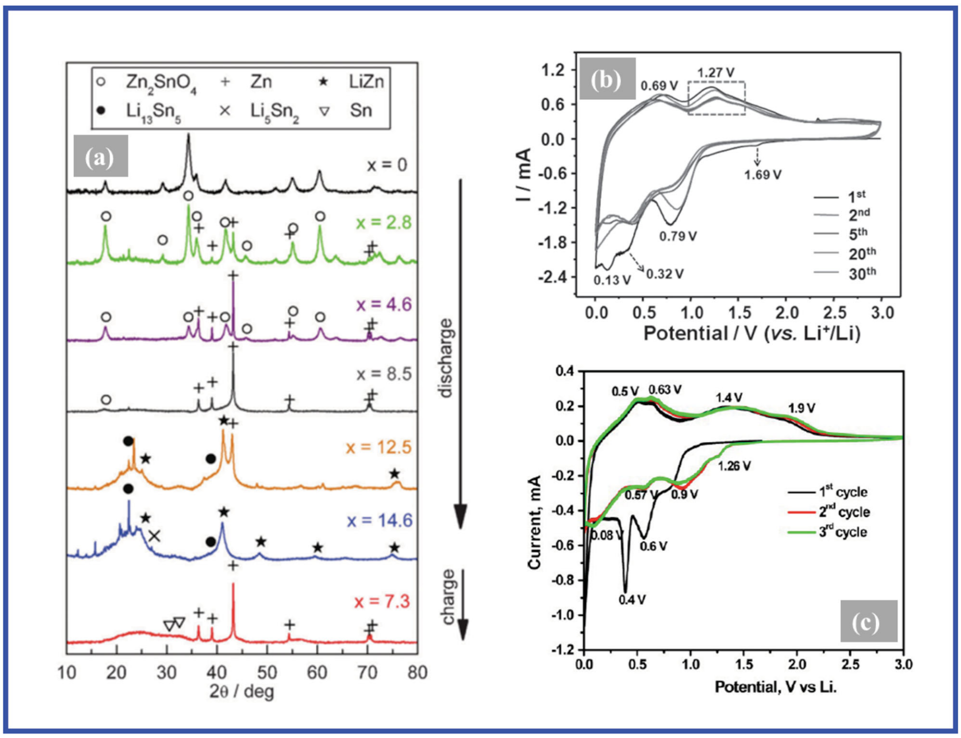

Figure 4. a) XRD patterns of mechano synthesized Zn_2SnO_4 at various states of charge. Reproduced with permission.[119] Copyright 2011, Royal Society of Chemistry. CV curves of b) $ZnSnO_3$@C composites, Reproduced with permission.[120] Copyright 2014, Wiley. and c) Zn_2SnO_4 nanowires. Reproduced with permission.[121] Copyright 2013, American Chemical Society.

structure of Zn_2SnO_4 was prepared with different amounts of alkaline mineralizer (NaOH).[116] The concentration of NaOH shows obvious effects on the particle size, morphology, and purity of the product of Zn_2SnO_4 particles, which further affects its electrochemical performance.[116] Zn_2SnO_4 particles with high purity, smaller particle size, and uniform morphology have the best properties for LIBs. The typical crystal structures of $ZnSnO_3$ and Zn_2SnO_4 are shown in **Figure 5**g and Figure 5h, respectively.

Furthermore, Chen and co-workers synthesized unique $ZnSnO_3$ nanocubes (ZSCs, Figure 5a) and $ZnSnO_3$ nanosheets (ZSSs, Figure 5b) via a dual-hydrolysis-assisted liquid precipitation reaction and subsequent hydrothermal route.[122] The capacity of the ZSS electrode decreased by 38.4% after 50 cycles, in contrast to a capacity decrease of 77.5% of the ZSC electrode. Two other kinds of zinc stannate cubes were compared as well, as shown in Figure 5c and d. First, monodisperse single crystal Zn_2SnO_4 cubes synthesized via a facile hydrothermal method[118] delivered a capacity of 775 mA h g^{-1} after 20 cycles at the current density of 50 mA g^{-1}. Second, in our previous research hollow Zn_2SnO_4 cubes were successfully synthesized via simple alkaline etching and a subsequent calcination process.[123] The hollow cubes showed good electrochemical performance (540 mA h g^{-1} after 45 cycles at the current density of 300 mA g^{-1}) and high rate capability. This significant improvement can be attributed to the hollow structure, which has a larger surface area and lower inner stress. It is concluded that the morphological structures of Zn_2SnO_4 highly affect the battery performance. To further confirm this point, a flower-like Zn_2SnO_4 composed of many rod-like protruding tips (Figure 5e)[124] also demonstrated satisfactory properties with a reversible capacity of 501 mAh g^{-1} over 50 cycles at the current density of 300 mA g^{-1}. Furthermore, similar to our previous study,[123] the double-shell and yolk-shell hollow amorphous $ZnSnO_3$ microcubes were developed. This structure can effectively releasing mechanical strain, keep the electrode integrity and provide enough space for buffering the volume change. As a result, it shows a better cycling stability with a high reversible capacity of 741 mA h g^{-1} after 50 cycles at 100 mA g^{-1}.

In addition, other approaches have been successfully employed to synthesize Zn_2SnO_4. For example, the Zn_2SnO_4 nanowires in Figure 5f were synthesized directly on a stainless steel substrate without any buffer layers by the vapor transport method.[121] This type of nanowire retains a capacity of 695 mAh g^{-1} over 60 cycles at the current density of 120 mAg^{-1}. Thus, designing unique and novel nanostructures of zinc stannate is an effective approach for improving performance.

Another approach is to introduce a buffering conductive matrix, like carbon,[229] metal oxide[230] or metal layer,[231] into the zinc stannate.[132] A thin porous carbon layer was used to modify the mesoporous and amorphous $ZnSnO_3$ nanocubes (see **Figure 6**a)[128] and delivered a high reversible capacity of 650 mA h g^{-1} at a very high rate of 3 A g^{-1}. This performance improvement originates from the advantages of small particle size, well-developed mesoporosity, the amorphous nature of $ZnSnO_3$ and the continuous conductive framework produced by the interconnected carbon layers. In our previous research, N-doped carbon coated Zn_2SnO_4 cubes were studied, and we

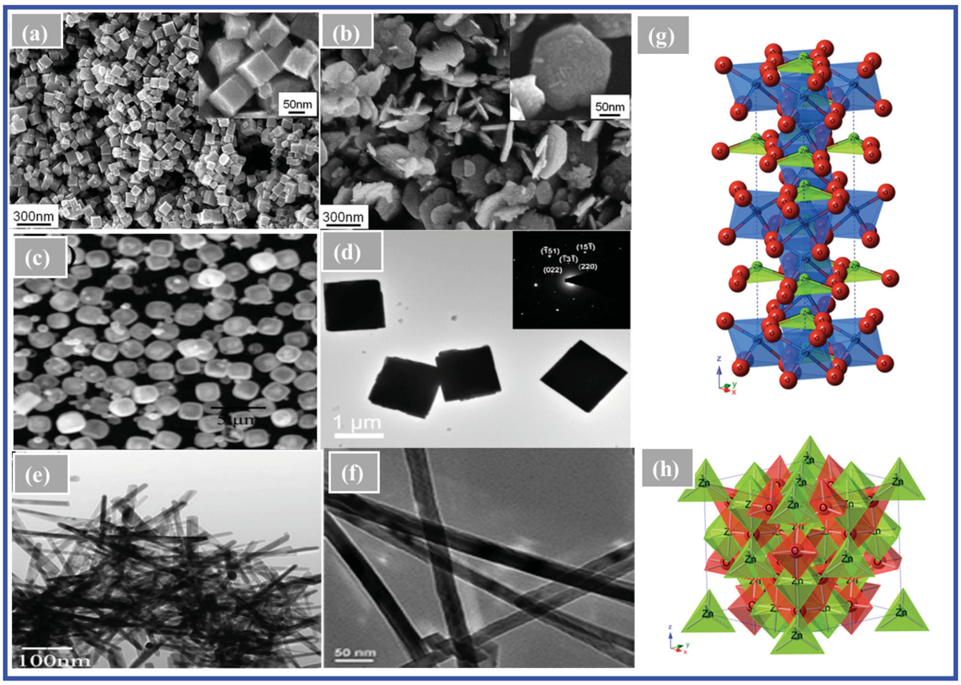

Figure 5. SEM images of a) $ZnSnO_3$ nanocubes, and b) $ZnSnO_3$ nanosheets. Reproduced with permission.[122] Copyright 2012, Royal Society of Chemistry. c) SEM images of Zn_2SnO_4 hollow boxe. Reproduced with permission.[123] Copyright 2013, Royal Society of Chemistry. d) TEM image of single crystal Zn_2SnO_4 cubes. Reproduced with permission.[118] Copyright 2012, Elsevier. e) TEM images of flower-like Zn_2SnO_4 composed of many rod-like tips protrude. Reproduced with permission.[124] Copyright 2014, Elsevier. f) TEM image of Zn_2SnO_4 nanowires. Reproduced with permission.[125] Copyright 2013, American Chemical Society. The crystal structure of f) $ZnSnO_3$, and h) Zn_2SnO_4.

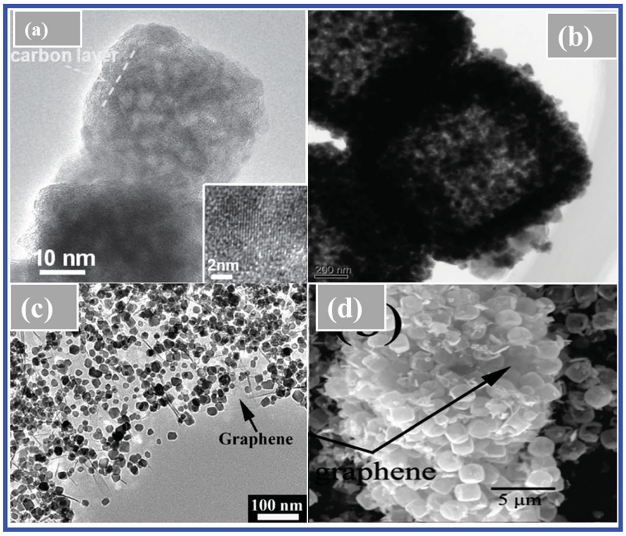

Figure 6. TEM images of a) thin porous carbon layer modified $ZnSnO_3$ nanocubes, b) N-doped carbon coated Zn_2SnO_4 cubes, and c) layered Zn_2SnO_4/graphene nanohybrids. a) Reproduced with permission.[128] Copyright 2014, Wiley. b) Reproduced with permission.[129] Copyright 2014, Elsevier. c) Reproduced with permission.[130] Copyright 2013, Elsevier. d) SEM image of Zn_2SnO_4/graphene composites. Reproduced with permission.[131] Copyright 2013, Royal Society of Chemistry.

demonstrated an enhanced electrochemical performance and high rate capability compared to the original cubes.[129] In this system, the N-doped carbon layer played an important role in buffering the volumetric change of the boxes and enhancing the ionic and electronic conductivities. Additionally, graphene has also been used as a conductive matrix for zinc stannate.[133] A facile in situ hydrothermal route was used to produce a layered Zn_2SnO_4/graphene nanohybrid[130] (see Figure 6c). In our studies, two kinds of Zn_2SnO_4/graphene composites were reported.[131,134] Both composites have similar morphologies, in which the hollow Zn_2SnO_4 boxes are supported or covered by flexible graphene nanosheets, resulting in enhanced electrochemical performance and high rate capability. Recently, a novel kind of co-doped Zn_2SnO_4–graphene–carbon nanocomposites exhibited a significantly higher reversible capacity of 699 mA h g^{-1} after 50 cycles at 100 mA g^{-1}.[135] This indicates that in addition to using highly conductive graphene nanosheets, doping is another significant factor that further increases electron transport and lithium ion diffusion.

Overall, zinc stannates have attracted more attention because of their unique properties and wide range of applications, especially for LIBs. The advantages of zinc stannates can be concluded as: a) The morphology and structures of zinc stannate are relatively easy to control. The nanostructures from 0D nanoparticles, 1D nanowires, 2D nanosheets, and 3D nanostructures exhibit great improvements to anode performance. b) In the first electrochemical reaction, additional Zn is produced, which can further alloy with lithium providing higher capacity. c) Compared with cobalt, zinc is much more environmentally friendly. For future research, hierarchical structures or multiple-buffering conductive matrices are suggested to enhance the cycling performance and rate properties by solving the serious volume change and relatively low conductivity problems.

2.4. Other Stannate Anodes

Other MSnOx (M = Ni, Sr, Ca, Mg et al.) materials have also been reported as anodes for LIBs.[136–139] **Table 1** summarizes the electrochemical performance of other metal stannate anodes. We firstly reported the electrochemical performance of $NiSnO_3$ compared with the mixture of NiO and SnO_2. It shows that the $NiSnO_3$ has better properties than the mixtures, which can be attributed to the initial products of NiO and Sn acting as 'self-matrices' for each other as well as the formed Li_2O matrix.[140] Subsequently, direct evidence of this conversion mechanism has been given. The TEM and SAED evidences indicate the obvious deposition process of $NiSnO_3$, that is, the formation of NiO, Sn and Li_2O at 0.9 V, decomposition of NiO at 0.6 V, followed by the alloy process of Sn. The distribution of the first step production of $NiSnO_3$ (NiO and Sn) is more homogeneous than mixtures resulting in the better performance as called 'self-matrixes'.

In this section, we have summarized the electrochemical reaction mechanisms, synthesis methods, nanostructure designs, and various nanohybrids of different types of stannates, which are an important class of MOMTs. Particularly, we emphasized three kinds of stannates based on the extensive research carried out on each: lithium stannates, cobalt stannates, and zinc stannates. In the first lithium insertion process, the $MSnO_x$ decomposes into three phases: Li_2O, Sn, and another metal, M. The extra metal or metal oxide produced from the first electrochemical reaction plays an important role in the following lithium intercalation/deintercalation processes. Among the several types of stagnates discussed above, lithium stannates show less advantages due to the low conductivity and

Table 1. Summary of the electrochemical performance of other metal stannate anodes for LIBs.

Materials	Feature	Electrochemical performance			Ref
		Current density [mAg^{-1}]	Cycle number	Capacity retention [mAh g^{-1}]	
$CaSnO_3$	Flower-like $CaSnO_3$	60	50	547	[138]
$CaSnO_3$	Porous $CaSnO_3$ nanotubes	60	50	565	[137]
$CaSnO_3$	Novel eggroll-like $CaSnO_3$ nanotubes	60	50	648	[136]
Mg_2SnO_4	Mg_2SnO_4/SnO_2 nanocomposites	60	20	350	[139]
$SrSnO_3$	$SrSnO_3$nanorods	50	50	200	[141]

inactive electrochemical properties of more Li_2O formation in the first discharge process. However, for other stannates like cobalt stannates, zinc stannates and nickel stannates, the metal (Co, Zn, Ni) or metal oxide (CoO, ZnO, NiO) can further react with Li or Li_2O as active materials as well as showing higher conductivity than Li_2O. In general, it not only acts as a soft matrix to buffer the volume expansion of Sn particles, but also provides some additional capacity. Another obvious advantage of MTMOs is that the formation of M or MO is in situ process during the electrochemical process, which is more uniform compared with the mixture of SnO_2 and MO. This kind of "self-matrix" system has a positive influence on the anode properties. However, the volume change and conductivity are still main issues for stannates. Many efforts and approaches have been attempted to solve these problems. One strategy is to make materials with novel nanostructures, like hollow or low-dimensional structures, which can effectively relieve the stress from volume expansion. Another popular way is to form a buffering conductive coating layer, such as carbon, graphene, or conductive polymers. Overall, the electrochemical performance of stannates can be dramatically enhanced after modifying their structures.

3. XMO_4 (M = Mo, Co, Fe, Mn)

3.1. Molybdates

In recent years, metal molybdates ($XMoO_4$) have been widely studied due to several oxidation states existing for these oxides, ranging from 3^+ to 6^+ for Mo,[34,39] which enhances the reversible capacity in LIB applications. $XMoO_4$ materials have also been applied in other research fields, such as tunable optical applications,[48,142] electrocatalysis,[40] and electrochemical capacitors.[73,140,143,144] $XMoO_4$ has been successfully synthesized via various methods, such as reverse microemulsion,[142] precipitation,[145,146] and hydrothermally.[49] For LIB applications, $XMoO_4$ can act as both cathode and anode materials. Lou et al. studied 1D $XMoO_4$ (X = Ni, Co) nanorods as cathode materials with a reversible capacity of 100 mA h g^{-1} after 70 cycles in the voltage window of 1.5–3.5 V.[147] Other a/b–$NiMoO_4$ cathode electrodes have been produced with a mesoporous honeycomb structure through polymer templating.[224] In this review, we mainly focus on $XMoO_4$ used as anodes for LIBs, which can have high reversible capacities at potentials less than 2.0 V.

The electrochemical reaction of $XMoO_4$ with lithium can be addressed as follows:

$$XMoO_4 + 8Li \rightarrow X + Mo + 4Li_2O$$

$$X + Li_2O \leftrightarrow XO + 2Li$$

$$Mo + 3Li_2O \leftrightarrow MoO_3 + 6Li$$

The reversible capacities are provided by the reaction between metal X and Mo with Li_2O. Thus, compared with just Mo oxide, these kind of molybdates show great potential as alternative anodes for LIBs due to the addition of metal X, which is electrochemically active and provides extra capacity.

Among $XMoO_4$ anodes, $CoMoO_4$ is the most promising for LIBs due to its high theoretical capacity of 980 mAhg^{-1}. $CoMoO_4$ has two crystalline structures, which are related to the atmospheric pressure. The low pressure structure (α-$CoMoO_4$) and the high pressure structure (β-$CoMoO_4$), along with $CoMoO_4 \cdot nH_2O$, have been studied.[148,149] Chowdari studied the interconnected network of α-$CoMoO_4$ sub-micrometer particles with the monoclinic crystal structure (shown in **Figure 7**e) and reported high reversible capacity as well as excellent capacity retention.[150] Subsequently, two kinds of $CoMoO_4$/graphene nanohybrids with different morphologies have been proposed. One is $CoMoO_4$ nanoparticles anchored on graphene ($CoMoO_4$ NP/RGO), shown in Figure 7a,[41] The other is $CoMoO_4$ nanorods distributed on graphene, which exhibited enhanced electrochemical performance.[39] The cycling performance of $CoMoO_4$ NP/RGO is shown in Figure 7b, demonstrating good rate capability and an impressive cycling stability of 920 mAhg^{-1}

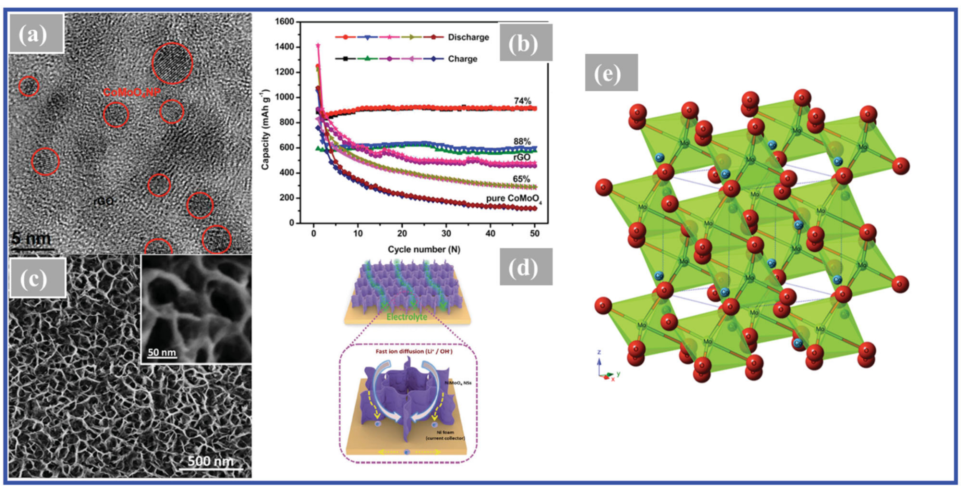

Figure 7. a) TEM image of $CoMoO_4$ NP/RGO, and b) cycling performance of $CoMoO_4$ NP/RGO with varying graphene content. Reproduced with permission.[41] Copyright 2014, American Chemical Society. c) SEM image of $NiMoO_4$ nanosheet arrays on Ni foam, and d) schematic showing the advantages of the hierarchical structure. Reproduced with permission.[72] Copyright 2015, Royal Society of Chemistry. e) The crystal structure of monoclinic $CoMoO_4$.

after 50 cycles. Synergetic chemical coupling effects between the graphene conductive network and nanoparticles leads to the significant impact on the performance. Similar to $CoMoO_4$, honeycomb-like $NiMoO_4$ nanosheet arrays have been synthesized via electrodeposition on Ni foam (Figure 7c).[72] It can be observed in Figure 7d that this reasonable design provides high surface area, short ion diffusion lengths, and effective electron transport pathways, further resulting in improved cycling and rate performance. A recent work reported that a type of phase-pure b-$NiMoO_4$ yolk–shell spheres can be obtained at pyrolysis temperature of 800 °C via one-pot spray pyrolysis.[232] In this design, the unique core/void/shell configuration with free space could better function to accommodate the volume change upon cycling. As a result, the pure phase $NiMoO_4$ yolk–shell spheres indicates much more higher capacity of 1292 mAhg^{-1} at 1000 mA g^{-1} compared with amorphous dense spheres and a/b-$NiMoO_4$ yolk–shell spheres.

3.2. Cobaltates

Co_3O_4 shows great research interest as anode materials for LIBs because of its high reversible capacity.[7] However, due to the toxicity and high cost of cobalt, many efforts have attempted to partially replace Co with other eco-friendly and low cost alternative elements.[51,151] To attain this goal, a series of promising studies on cobaltates (MCo_2O_4) for LIB anodes has been reported.

$ZnCo_2O_4$ is the most popular cobaltate studied. As shown in **Figure 8**a, bivalent Zn-ions occupy the tetrahedral sites in the cubic spinel structure and the trivalent Co-ions occupy the octahedral sites.[151,152] In this case, the Zn can provide additional capacity due to the alloying process between Zn and Li, which is not a complete conversion reaction as with cobalt oxides. It can be explained by the electrochemical reaction of $ZnCo_2O_4$:[4]

$$ZnCo_2O_4 + 8Li^+ + 8e^- \leftrightarrow Zn + 2Co + 4Li_2O$$

$$Zn + Li^+ + e^- \leftrightarrow LiZn$$

$$Zn + Li_2O \leftrightarrow ZnO + 2Li^+ + 2e^-$$

$$2Co + 2Li_2O \leftrightarrow 2CoO + 4Li^+ + 4e^-$$

$$2CoO + 2/3Li_2O \leftrightarrow 2/3Co_3O_4 + 4/3Li^+ + 4/3e^-$$

It is clear that the reaction mechanism of $ZnCo_2O_4$ is complex and involves multiple steps due to the multielement formation. The first reaction is irreversible, producing Zn, Co, and Li_2O. The metal Zn and Co can then further react with Li_2O in the following conversion reactions. These reactions are illustrated by the typical CV curves of $ZnCo_2O_4$, shown in Figure 8b.[152] In the first cycle, the peak at 0.67 V in the cathodic process corresponds to the decomposition of $ZnCo_2O_4$. Due to the different electrochemical mechanisms, this cathodic peak may move to 1.1 V. In the first and following cycles, two oxidation peaks at 1.7 V and 2.2 V can be assigned to the reaction of Zn to Zn^{2+} and Co to Co^{3+}, respectively.[153] Other kinds of cobaltates, such as $NiCo_2O_4$,[154] $MnCo_2O_4$,[155] and $FeCo_2O_4$,[156] exhibit similar electrochemical mechanisms to $ZnCo_2O_4$.

Many researchers have attempted to design various $ZnCo_2O_4$ nanostructures with different dimensions. 1D $ZnCo_2O_4$ nanowires

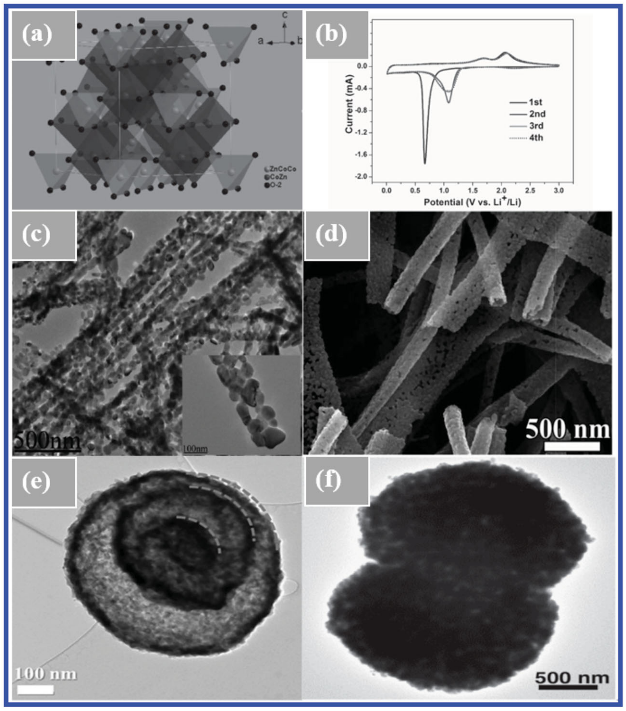

Figure 8. a) The crystal structure of spinel $ZnCo_2O_4$, and b) the CV curve of $ZnCo_2O_4$ twin microspheres. Reproduced with permission.[152] Copyright 2014, Wiley. c) TEM image of $ZnCo_2O_4$ nanowires. Reproduced with permission.[157] Copyright 2011, American Chemical Society. d) SEM image of porous $ZnCo_2O_4$ nanotubes. Reproduced with permission.[158] Copyright 2012, Royal Society of Chemistry. TEM image of e) yolk-shell hollow $ZnCo_2O_4$ powders, Reproduced with permission.[152] Copyright 2014, Wiley. and f) $ZnCo_2O_4$ twin microspheres. Reproduced with permission.[159] Copyright 2013, Wiley.

composed of nanocrystals have been proposed, as shown in Figure 8c.[157] Another 1D porous $ZnCo_2O_4$ nanotube structure with diameters of 200–300 nm and lengths up to several millimeters with a hollow interior has been studied (Figure 8d). Both 1D nanostructures can provide high surface-to-volume ratios and excellent electronic transport properties, which are expected to enhance LIB capacity and cycling performance.[158] In addition to 1D nanostructures, a number of research focuses on building 3D nanostructures with high surface area, low density, and high loading capacity.[233–235] For instance, uniform mesoporous $ZnCo_2O_4$ microspheres were reported to maintain a reversible capacity of 721 mAhg^{-1} after 80 cycles.[4] An interesting study focused on $ZnCo_2O_4$ mesoporous twin microspheres and microcubes (Figure 8f).[152] As with other MTMOs, the volume expansion of $ZnCo_2O_4$ is still the main issue and the research results demonstrate that a hollow structure or yolk-shell arrangement are promising approaches to solve this problem.[235,236] Thus, some yolk-shell $ZnCo_2O_4$ spheres have been reported in recent years.[159–161] For example,[159] a single-crystal yolk-shell hollow $ZnCo_2O_4$ sphere with three layers can be observed in Figure 8e. The voids between the yolk and the shell can serve as buffering spaces for the electroactive core material during lithium insertion and extraction.[159] Controlling the nanostructure is considered an effective strategy for other kinds of cobaltates, in which a series of studies have been performed for $NiCo_2O_4$,[162–173,237] $FeCo_2O_4$,[156] and $MnCo_2O_4$.[174,238]

Researchers have stated that the simple structures of $ZnCo_2O_4$ may still suffer from poor electronic conductivity and volume expansion during lithium intercalation/deintercalation, leading to rapid capacity fading.[175] 3D hierarchical nanostructures using high conductivity free-standing current collectors have been designed for highly flexible LIBs with excellent mechanical strength on carbon cloth,[175]carbon fibers,[176,177] graphene foam,[239] and Ni foam.[64,178–180,240] For instance, 3D hierarchical $ZnCo_2O_4$ nanowire arrays were deposited on carbon cloth (**Figure 9**a), where the fibers had a uniform diameter of approximately 20 µm. This design delivered a specific capacity of 1200 mAhg^{-1} after 160 cycles (Figure 9b).[175] A similar structure of $ZnCo_2O_4$ nanowires on Ni foam was also proposed. The nanowires had uniform diameters of 80–100 nm and lengths of about 5 mm (Figure 9d,e). Benefiting from the hierarchical structure, this free-standing $ZnCo_2O_4$ nanocomposite showed high reversible capacity and rate capability, as well as stable cycling performance. The schematic illustration of the operating principles of $ZnCo_2O_4$ nanowire array/carbon cloth composites (Figure 9c) helps explain this hierarchical structure. This nanostructure provides outstanding electronic conductivity, short Li-ion diffusion paths, and ideal conditions for facile diffusion of the electrolyte, in addition to accommodating the strain induced by large volume changes.[175] In addition, other nanostructures have been proposed to increase anode performance. A high capacity of 960.8 mAhg^{-1} over 100 cycles was obtained by a hierarchical hybrid structure of rGO-supported $ZnCo_2O_4$ nanosheets.[181] Similarly, rGO/$NiCo_2O_4$ nanosheet nanocomposites were synthesized via the method illustrated in **Figure 10**a.[182] The resultant morphology contains numerous ultrathin nanosheets grown on GO (Figure 10b) and resulted in stable cycling performance of 954.3 mAhg^{-1} after 50 cycles (Figure 10c).

Metal organic frameworks (MOFs) have recently received a lot of attention due to their unique properties such as high surface areas and porosity.[184] It has been reported that MOFs can be used as a precursor or sacrificial template to construct metal oxides or metals coated with carbon for LIBs.[185–188,241] Interestingly, porous $Zn_xCo_{3-x}O_4$ hollow polyhedra composed of nanosized building blocks were synthesized from heterobimetallic zeolitic imidazolate frameworks (ZIFs).[183] **Figure 11**a illustrates the synthesis of bimetallic ZIFs and their conversion to spinel $Zn_xCo_{3-x}O_4$ hollow polyhedra. The $Zn_xCo_{3-x}O_4$ hollow polyhedra (Figure 11b) exhibited excellent reversible capacities as high as 990 mAhg^{-1} with excellent stability after 50 cycles (Figure 11c). Another sandwich structure of RGO wrapped $ZnCo_2O_4$–ZnO–C polyhedrons on nickel foam derived from ZIFs has been reported very recently.[242] In the composites, the open pores inherited from ZIF provide sufficient contact area with electrolyte, and serve as cushion space for volume changes. The RGO nanosheets act as a flexible protector to mixed metal oxides, and Ni foam act as the high conductive substrate. In this case, as-prepared RGO/$ZnCo_2O_4$–ZnO–C/Ni sandwich-structured exhibit superior Coulombic efficiency, excellent cycling stability and rate capability.

In conclusion, cobaltates may be a better choice as substitutes for Co_3O_4 because of their lower toxicity and high capacities. Compared with Co_3O_4, the additional metal elements, such as Zn, Fe or Mn, have positive effects on the electrochemical reactions. The reason is the conversion reaction or alloying/de-alloying reaction of M with Li_2O, which can further increase the capacity compared to that of only Co_3O_4. However, the conductivity and volume exchange of this kind of MTMOs are still the main limits to the performance. To solve these problems, researchers should focus on the design of nanostructured cobaltates, as well as hierarchical structures with highly conductive substrates like carbon cloth, Ni foam, or graphene nanosheets.

3.3. Ferrites

Ferrites (MFe_2O_4), as alternative anode materials to iron oxides, have been studied for their application in LIBs. Fe_3O_4 offers a theoretical capacity of 926 mAhg^{-1}, assuming the completely reversible formation of four Li_2O per formula unit.[189] In comparison, the theoretical capacity of $ZnFe_2O_4$

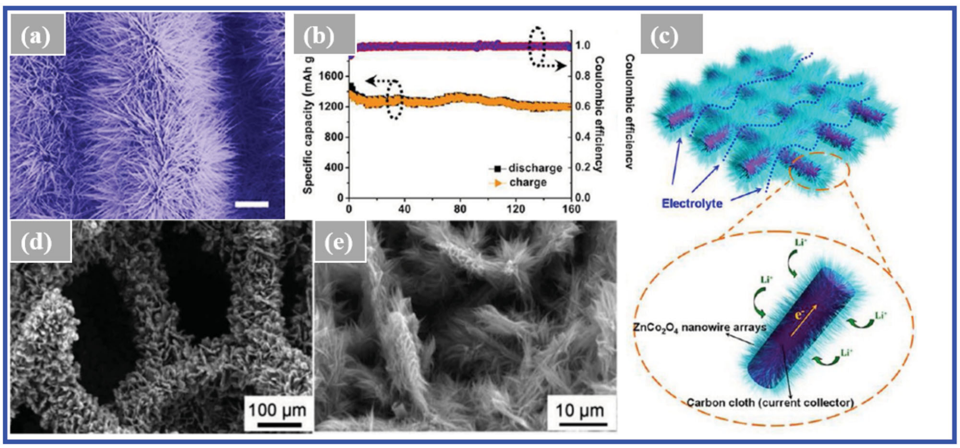

Figure 9. a) SEM image, b) cycling performance, and c) schematic representation and operating principles of $ZnCo_2O_4$ nanowire arrays/carbon cloth composites. Reproduced with permission.[175] Copyright 2012, American Chemical Society. d,e) SEM image of $ZnCo_2O_4$ nanowires on Ni foam. Reproduced with permission[178] Copyright 2014, Royal Society of Chemistry.

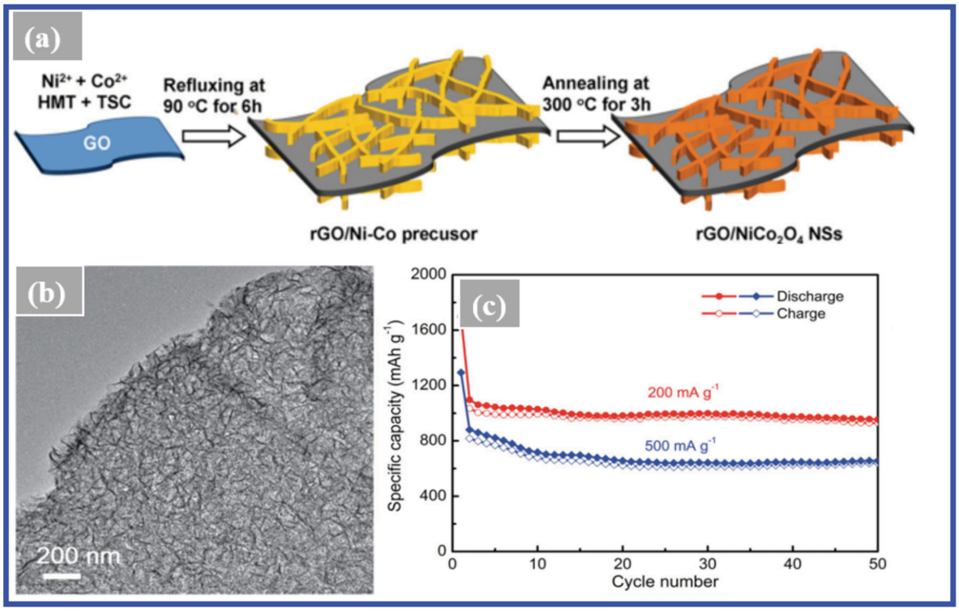

Figure 10. a) Schematic illustration of the formation of rGO/$NiCo_2O_4$ nanosheets nanocomposite through a facile solution growth and a subsequent thermal annealing treatment in air, b) TEM image of rGO/$NiCo_2O_4$ composites, and c) cycling performance at two current densities. Reproduced with permission.[182] Copyright 2015, Wiley.

can reach 1000.5 mAh g^{-1} according to the reversible reaction of Zn with Li or Li_2O, involving nine Li ions per formula unit of $ZnFe_2O_4$. The investigation of the lithiation–delithiation kinetics of carbon-coated $ZnFe_2O_4$ nanoparticles was reported by Belmonte et al.[190] They confirmed that the first lithiation of $ZnFe_2O_4$ nanoparticles is a multistep process involving the presence of intermediate Li–Zn–Fe–O phases as precursors for the formation of amorphous Li_2O and the following reaction to

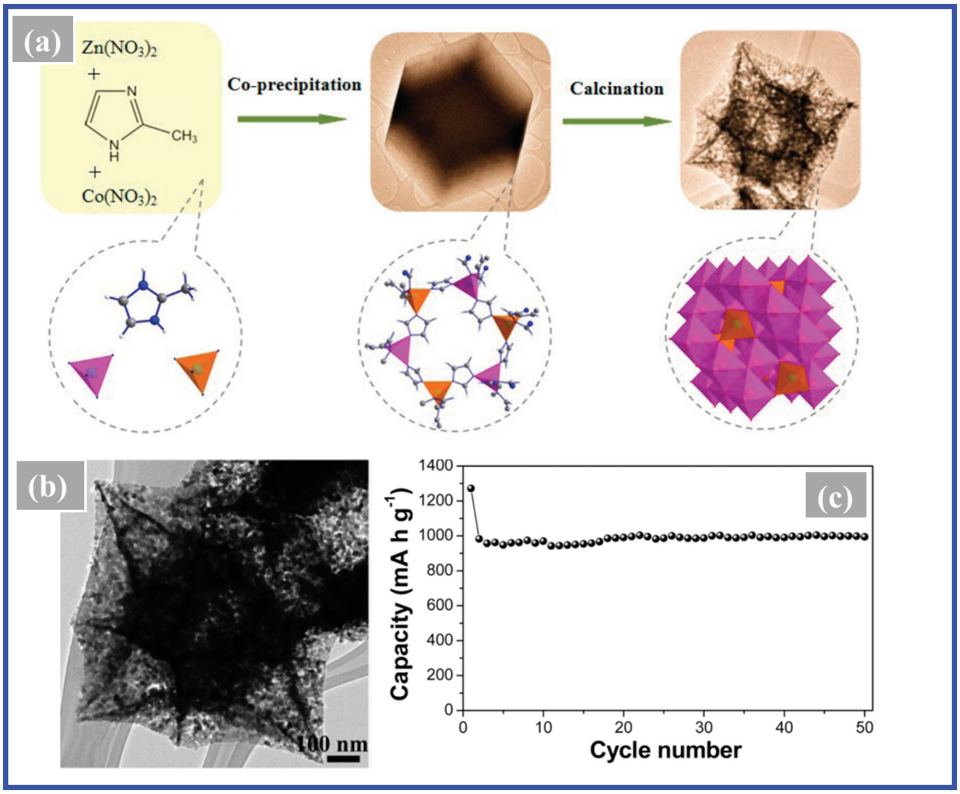

Figure 11. a) Schematic illustration of the preparation of bimetallic ZIFs and their conversion to spinel $Zn_xCo_{3-x}O_4$ hollowpolyhedra. b) TEM image, and c) cycling performance of $Zn_xCo_{3-x}O_4$ hollowpolyhedra. Reproduced with permission.[183] Copyright 2014, American Chemical Society.

produce highly dispersed LiZn and Fe in an amorphous Li_2O matrix. For ferrites (MFe_2O_4), the metal M can be Ni, Co, or Cu.

A lot of research for MFe_2O_4 has focused on developing different dimensional nanostructures.[71,195,196,243] Porous 1D $NiFe_2O_4$ nanofibers with an average diameter of 250 nm were successfully prepared via electrospinning, as seen in **Figure 12**c.[193] Porous 2D $CoFe_2O_4$ nanosheets with a thickness of 30–60 nm and lateral size of several micrometers (Figure 12d) have also been reported.[194] Surprisingly, these kinds of $CoFe_2O_4$ nanosheets exhibit a superior reversible capacity of 1147 mA h g^{-1} after 30 cycles and stable cycling performance. Subsequently, various 3D nanostructures of MFe_2O_4 have also been reported, like spheres,[197–199] cubes,[200] and ordered macroporous,[201] and yolk-shell structures. A simple spray drying process has been used to synthesize yolk-shell $ZnFe_2O_4$ powders,[192] TEM images in Figure 12e and f show the novel structure, with a minimum of two shells in each particle separated by an inner void. This kind of structure functions well for MFe_2O_4, as well as $ZnCo_2O_4$ discussed above, because it provides buffering spaces for the electroactive core material and improves the surface area. The typical crystal structure of $ZnFe_2O_4$ along the 112 direction in Figure 12a gives rise to some of the advantages of this anode material. The spinel 3D $ZnFe_2O_4$ octahedrons in Figure 12b were reported to show an excellent specific capacity of 910 $mAhg^{-1}$ after 80 cycles. These properties are suggested to enhance the surface areas, shorten lithium transport distances, and create a volume-change buffering system. However, another issue is the conductivity of MFe_2O_4. Many efforts have attempted to solve this problem. Carbon materials, such as carbon,[189,202] N-doped carbon,[244] carbon nanotubes,[203] and graphene,[69,204–209] or other conductive materials, like conductive polymers,[245] are great candidates due to their high conductivity and stability. After introducing carbon nanomaterials into the MFe_2O_4 structure, the electrochemical performance is rapidly improved, attributed to the highly conductive and buffering matrix of the carbons.

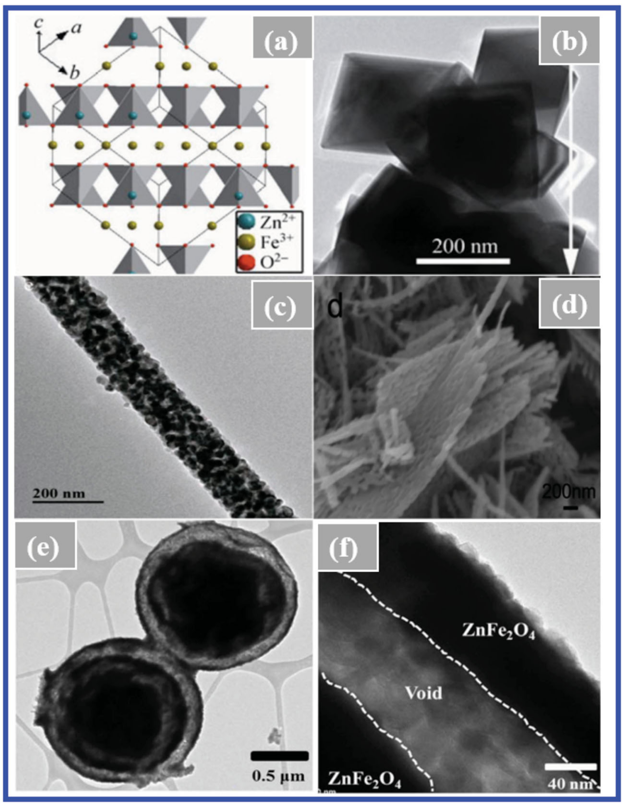

Figure 12. a) Lattice fringes of $ZnFe_2O_4$ octahedron. Reproduced with permission.[191] Copyright 2012, Springer. TEM image of b) typical $ZnFe_2O_4$ octahedron, Reproduced with permission.[191] Copyright 2012, Springer. c) $NiFe_2O_4$ nanofibers,Reproduced with permission.[192] Copyright 2014, Nature Publishing Group, and e,f) yolk-shell structured $ZnFe_2O_4$ powders. Reproduced with permission.[193] Copyright 2014, Springer. d) SEM image of $CoFe_2O_4$ nanosheets. Reproduced with permission.[194] Copyright 2014, Royal Society of Chemistry.

MOFs are effective sacrificial templates or precursors for the synthesis of MFe_2O_4 and its composites. As shown in **Figure 13**a, hierarchical $NiFe_2O_4/Fe_2O_3$ nanotubes were synthesized by Fe/Ni-based MOFs.[210] Figure 13b reveals that the hierarchical nanocomposites consist of nanotubes with diameters of 78 nm and lengths of about 1 µm. The composites show a reversible specific capacity of 936.9 $mAhg^{-1}$ up to 100 cycles (Figure 13c). Another method is to use MOFs as precursors for nanoporous carbon structures involving well-connected carbon networks in MTMOs. Huang et al. reported novel porous $ZnO/ZnFe_2O_4/C$ octahedra with hollow interiors fabricated using a MOF as both the precursor and the self-sacrificing template[211] (Figure 13d). In this case, the nanocrystals are embedded in a 3D interconnected, porous carbon framework. Even after 100 cycles, the

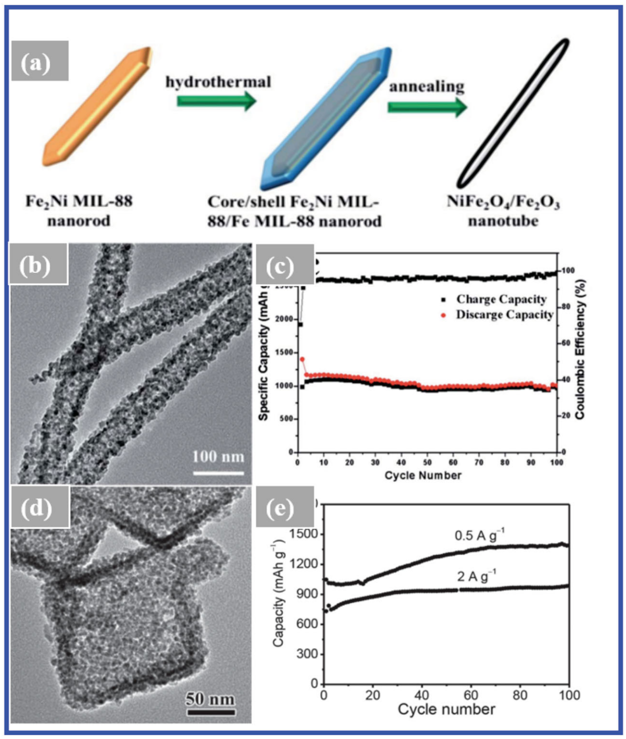

Figure 13. a) Schematic illustration of the procedure used to fabricate $NiFe_2O_4/Fe_2O_3$ nanotubes. b) TEM image, and c) cycling performance of $NiFe_2O_4/Fe_2O_3$ nanotubes. Reproduced with permission.[210] Copyright 2014, Royal Society of Chemistry. d) TEM images, and e) cycling properties of porous $ZnO/ZnFe_2O_4/C$ hollow octahedra. Reproduced with permission.[211] Copyright 2014, Wiley.

nanocomposites still maintain a superior reversible capacity of 1390 mAh g^{-1} (Figure 13e). Lately, using prussian blue as the self-sacrificial template, a general method was reported to synthesize porous hollow spinel AFe_2O4 nanoarchitectures.[246] Via this general approach, some hollow boxes of $NiFe_2O_4$, $ZnFe_2O_4$, and $CoFe_2O_4$ were successfully fabricated. In this designed structure, a short diffusion distance can be achieved by the porous frameworks and hollow interior derived from MOFs. In particular, $NiFe_2O_4$ hollow box exhibits high specific capacities of 841 mA h g^{-1} after 100 cycles at current densities of 1.0 A g^{-1}. It clearly shows that MOFs as a template can be extended to design porous carbon-stabilized metal oxide or MTMO electrode materials with superior specific capacity and stable cycling properties.

3.4. Manganates

Among the MTMOs, manganates (XMn_2O_4) have the advantages of low toxicity, low cost, and reasonably low operating voltages (0.5 V for charging and 1.2 V for discharging) compared with Co and Fe.[212–214,247] Lower charge/discharge voltages of the anode materials can effectively increase the energy density of LIBs. Thus, XMn_2O_4 attracts more and more attention from researchers and many studies have been performed to focus on these types of anode materials.[215–218,248]

1D nanomaterials, such as nanowires and nanotubes, can supply fast Li^+ and electron transport pathways, large contact area with electrolyte, and a buffer zone for mechanical stress during electrochemical processes. Thus, 1D manganates show great interests. For instance, 1D porous $ZnMn_2O_4$ nanowires[249] and hollow $ZnMn_2O_4$ nanotubes[250] have been demonstrated with obvious advantages. Both of the 1D nanostructures indicate superior electrochemical lithium-storage performance with a high specific capacity, good rate behavior, and excellent cyclability, which can be attributed to the unique 1D structure.

Lou' group has already synthesized a series of XMn_2O_4 materials as anodes for LIBs, such as $CoMn_2O_4$ nanowire arrays and $MnCo_2O_4$ nanosheet arrays grown on stainless steel, as seen in **Figure 14**d and Figure 14e, respectively.[219] Some other nanostructures, such as $ZnMn_2O_4$ hollow microspheres[220] (Figure 14b), $ZnMn_2O_4$ ball-in-ball hollow microspheres[221] (Figure 14g, crystal structure of tetragonal shown in Figure 14h), and double-shelled $CoMn_2O_4$ hollow microcubes (Figure 14f),[222] have also been reported by his group. These novel structures provide a great buffering matrix that alleviates the pulverization problem, making the electrode stable and enhancing the cycling performance.

Another interesting work has been reported by Chen et al., who fabricated a hierarchical mesoporous structure of $CoMn_2O_4$.[223] The $CoMn_2O_4$ microspheres consist of mesoporous nanosheets, in which the open spaces between neighboring nanosheets can be observed in Figure 14b. The schematic illustration of the diffusion of electrolyte, electrons, and Li ions in Figure 14a demonstrates the advantages of this hierarchical structure; it provides enhanced contact area with the electrolyte, shortens the Li-ion diffusion length in the nanosheets, and relieves strain from volume expansion. As a result, this hierarchical structure results in a high discharge capacity of 894 mAh g^{-1} after 65 cycles (Figure 14c).

In this section, we discuss the design, fabrication and application of XMO_4 materials as anode materials for LIBs, emphasizing four types of it, including molybdates, cobaltates, ferrites, and manganates. They all can indicate quite high electrochemical performances with rational design. Among these systems, XMO_4 and XMn_2O_4 show greater potential as anode materials for LIBs compared with others. The advantages can be attributed to the lower charge/discharge voltages leading to high energy density and environmental friendly compared with Co. Generally, the electrochemical reactions of XMO_4 during the conversion process with lithium can be marked as:

$$XM_2O_4 + Li^+ + e^- \rightarrow X + M + Li_2O$$

$$X + Li_2O \rightarrow XO + Li^+ + e^-$$

$$M + Li_2O \rightarrow MO + Li^+ + 4e$$

The initial reaction is always considered as the irreversible process that produces two different metal and Li_2O from XMO_4. The major reversible capacities are from the following conversion reaction between two types of metal and Li_2O. In this case, highly dispersed metal M and X can be obtained in an amorphous Li_2O matrix and each of them can serve as ''self-matrices'' for others, which can achieve better electrochemical performances than TMOs. However, as metal oxides for conversion mechanism, these kinds of materials still suffer from the serious volume change and conductivity issues. Two popular approaches are attempted for XMO_4, which are designing unique nanostructure and manufacture of composites with high conductive matrix. More recently, 3D free-standing nanostructures and materials derived from MOFs attract increasing attention in building high performances XMO_4, which we have discussed in detail for four different types materials.

4. Summary and Outlook

In this review, we summarized the recent development and understanding of novel MTMOs as anode materials for LIBs, including stannate, molybdates, cobaltates, ferrites, and manganates. Firstly, the electrochemical mechanisms of these materials were discussed in detail. The initial reaction of MTMOs is an irreversible process corresponding to the decomposition of MTMOs into multiple metals and/or metal oxides. Compared with traditional metal oxides, the additional metals or metal oxides from MTMOs function as ''self-matrices'' for each other besides the formed Li_2O matrix. Furthermore, extra metals or metal oxides with additional electrochemical activities can interact with Li ions via alloying/de-alloying or conversion reactions to deliver higher reversible capacities. However, similar to the mechanisms of alloying/de-alloying and conversion reactions, the main problems of MTMOs during lithium insertion/extraction are the serious volume changes and relatively low conductivity. As we discussed, several strategies are applied to boost the electrochemical performance. One of the most promising strategies is to design nano/microstructures with different dimensions containing various unique features. Some hierarchical structures or free-standing structures were explored to further achieve more structural stability.

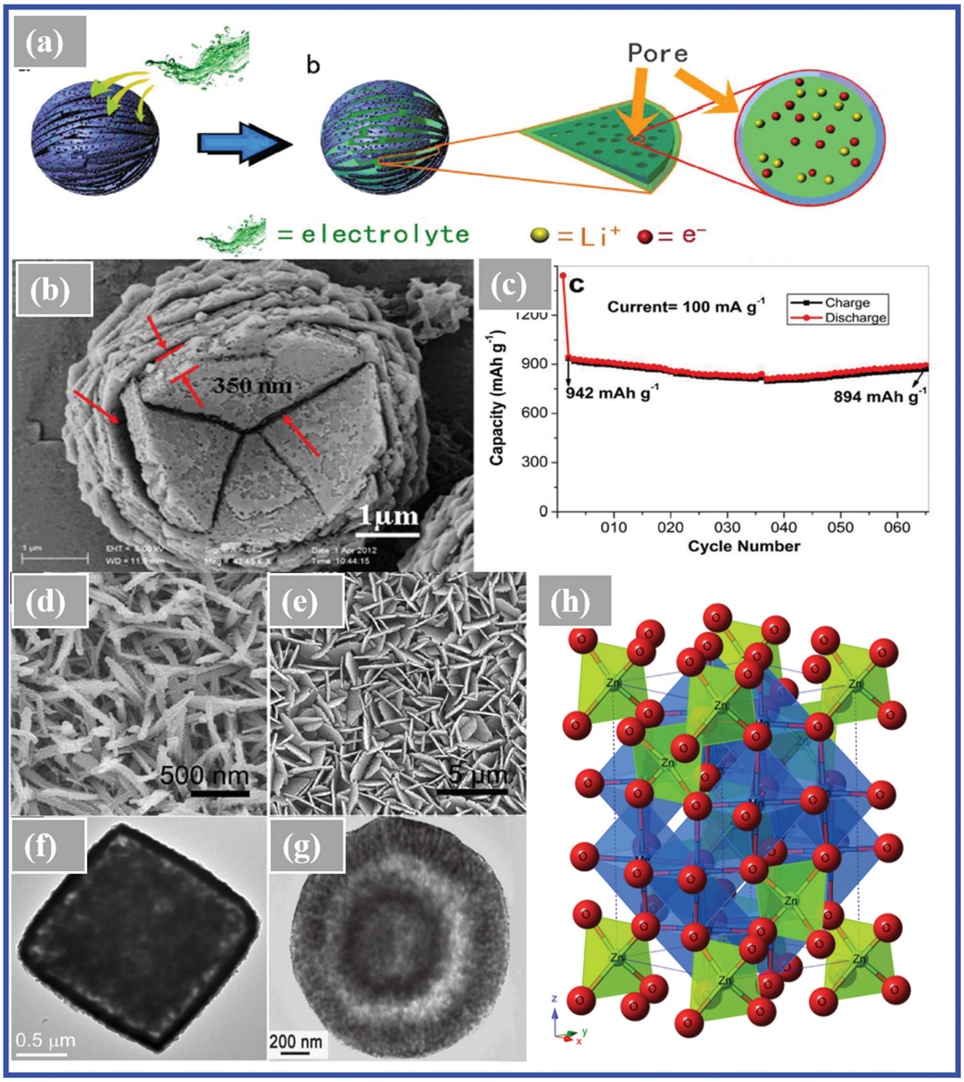

Figure 14. a) Schematic illustration of the electrochemical reaction, b) SEM image, and c) cycling performance of $ZnMn_2O_4$ microspheres. Reproduced with permission.[223] Copyright 2012, Nature Publishing Group. SEM image of d) $Co_xMn_{3x}O_4$ nanowire array and e) nanosheet array. Reproduced with permission.[219] Copyright 2013, Royal Society of Chemistry. f) TEM images of hollow $CoMn_2O_4$ nanocube, Reproduced with permission.[222] Copyright 2012, Royal Society of Chemistry. and g) yolk-shell $CoMn_2O_4$ nanospheres. Reproduced with permission.[221] Copyright 2012, Wiley. h) The crystal structure of tetragonal $ZnMn_2O_4$.

Although significant results have been achieved using MTMOs as anode materials for LIBs, there are still challenges to be overcome in the future. The specific capacity and cycle life of MTMOs need to be further improved to satisfy the requirements of high electrochemical performance. Firstly, controllable fabrication of the structure and morphology of MTMOs is still required. For instance, MTMOs derived from MOFs could be an effective strategy for fabrication of porous, hollow, even hierarchical nanostructure with formation of carbon matrix. Due to the unique properties of MOFs, more studies should be done to adjust the morphology, pore sizes and surface areas, which further determine both structure and battery performance of MTMOs.[254] As we know, the unique morphologies exhibit significant influence on the electrochemical performance of MTMOs. Some types of MTMOs have been explored with different novel structures and morphologies. However, the correlations between their various structures and battery performance need to be understood to design the optimized nanostructures with enhanced cycling performance. Furthermore, the exploitations of novel nanostructured MTMOs, such as hollow, core–shell, and yolk–core, especially for stannate, are still needed more efforts. Secondly, the doping strategy can be effectively applied to enhance LIB performance of active materials. It is believe that appropriate doping elements of MTMOs can assist to achieve a higher electronic conductivity and faster lithium ion diffusivity due to increased free electron concentration. Meanwhile, using bigger atoms to replace small atoms can provides larger space for the movement of lithium ions. However, very few report focus on the doping of MTMOs. It is expected to be a valuable approach to enhance the conductivity of semi-conducting MTMOs with higher rate performances. Thirdly, some interfacial reactions are some of the most serious

REVIEW

problems between the electrode and liquid electrolyte in LIBs. SEI film on the anode materials can consume lithium ions permanently, leading to reduced Columbic efficiency of batteries, which also exists in MTMOs. Thus, surface modification and coating on MTMOs is proposed to reduce the undesired side reactions and obtain improved electrochemical performances of MTMOs. In particular, an atomic layer deposition, which has been extensively studied by our group for modification of different types of anode and cathode materials,[251,252] is considered as the advanced coating technique to ameliorate the surface of MTMO with precisely tuned thickness and uniform coating layers. Fourthly, rational hybrid design of MTMOs is expected to be another effective approach for achieving high performances and stability. Meanwhile, introducing of conductive substrate for MTMOs is promising for fabrication of flexible energy storage devices. In addition, similar with MTMOs, mixed transition metal sulfides (MTMSs) are attracting increasing attention in LIBs or other energy storage device due to some obvious advantages of an 10^4 times higher electric conductivity than conventional MO semiconductors.[253] However, the electrochemical mechanism of MTMSs has not been clearly understood. In this case, analogical methods to optimize both the synthesis parameters, material properties and electrochemical mechanism of MTMOs can be switch over to MTMSs to study some fundamental understanding, which will be another interesting topic and further expand the potential materials for high performances LIBs.

In general, MTMOs belong to a novel research topic, and further studies are required to optimize battery performance. With rational and careful design, it is expected that MTMOs with various structures and morphologies will become one of the promising candidates as anode materials for next-generation high performance LIBs.

Acknowledgments

This research was supported by the National Natural Science Foundation of China (51572194), the Key Projects of Tianjin Municipal Natural Science Foundation of China (14JCZDJC32200 and 13JCZDJC33900), LPMT (Laboratory of Precision Manufacturing Technology), CAEP (KF14006), Academic Innovation Funding of Tianjin Normal University (52XC1404), Training Plan of Leader Talent of University in Tianjin, the program of Thousand Youth Talents in Tianjin of China, Nature Sciences and Engineering Research Council of Canada (NSERC) and Canada Research Chair (CRC) Program.

Received: November 3, 2015
Revised: December 15, 2015
Published online: February 9, 2016

[1] J.-M. Tarascon, M. Armand, *Nature* **2001**, *414*, 359.
[2] M. Armand, J.-M. Tarascon, *Nature* **2008**, *451*, 652.
[3] P. G. Bruce, B. Scrosati, J. M. Tarascon, *Angew. Chem* **2008**, *47*, 2930.
[4] L. Hu, B. Qu, C. Li, Y. Chen, L. Mei, D. Lei, L. Chen, Q. Li, T. Wang, *J. Mater. Chem. A* **2013**, *1*, 5596.
[5] H. B. Wu, J. S. Chen, H. H. Hng, X. W. Lou, *Nanoscale* **2012**, *4*, 2526.
[6] A. S. Aricò, P. Bruce, B. Scrosati, J.-M. Tarascon, W. Van Schalkwijk, *Nat. Mater.* **2005**, *4*, 366.
[7] X. Su, Q. Wu, J. Li, X. Xiao, A. Lott, W. Lu, B. W. Sheldon, J. Wu, *Adv. Energy Mater.* **2014**, *4*, 1300882.
[8] G. Chen, J. Yang, J. Tang, X. Zhou, *RSC Adv.* **2015**, *5*, 23067.
[9] H. Zhou, *Energy Environ. Sci.* **2013**, *6*, 2256.
[10] H. Chang, H. Wu, *Energy Environ. Sci.* **2013**, *6*, 3483.
[11] P. Poizot, S. Laruelle, S. Grugeon, L. Dupont, J. Tarascon, *Nature* **2000**, *407*, 496.
[12] K. T. Lee, Y. S. Jung, S. M. Oh, *J. Am. Chem. Soc.* **2003**, *125*, 5652.
[13] Y. Wu, E. Rahm, R. Holze, *J. Power Sources* **2003**, *114*, 228.
[14] L. Ji, Z. Lin, M. Alcoutlabi, X. Zhang, *Energy Environ. Sci.* **2011**, *4*, 2682.
[15] H. Kim, J. Cho, *J. Mater. Chem.* **2008**, *18*, 771.
[16] X. W. Lou, Y. Wang, C. Yuan, J. Y. Lee, L. A. Archer, *Adv. Mater.* **2006**, *18*, 2325.
[17] M. S. Park, G. X. Wang, Y. M. Kang, D. Wexler, S. X. Dou, H. K. Liu, *Angew. Chem.* **2007**, *119*, 764.
[18] C. Wang, Y. Zhou, M. Ge, X. Xu, Z. Zhang, J. Jiang, *J. Am. Chem. Soc.* **2009**, *132*, 46.
[19] R. Demir-Cakan, Y.-S. Hu, M. Antonietti, J. Maier, M.-M. Titirici, *Chem. Mater.* **2008**, *20*, 1227.
[20] W.-Y. Li, L.-N. Xu, J. Chen, *Adv. Funct. Mater.* **2005**, *15*, 851.
[21] X. W. Lou, D. Deng, J. Y. Lee, J. Feng, L. A. Archer, *Adv. Mater.* **2008**, *20*, 258.
[22] Y. Li, B. Tan, Y. Wu, *Nano Lett.* **2008**, *8*, 265.
[23] X. W. Lou, D. Deng, J. Y. Lee, L. A. Archer, *J. Mater. Chem.* **2008**, *18*, 4397.
[24] B. Varghese, M. Reddy, Z. Yanwu, C. S. Lit, T. C. Hoong, G. Subba Rao, B. Chowdari, A. T. S. Wee, C. T. Lim, C.-H. Sow, *Chem. Mater.* **2008**, *20*, 3360.
[25] S. A. Needham, G. Wang, H. K. Liu, *J. Power Sources* **2006**, *159*, 254.
[26] H. Liu, G. Wang, J. Liu, S. Qiao, H. Ahn, *J. Mater. Chem.* **2011**, *21*, 3046.
[27] L. Liu, Y. Li, S. Yuan, M. Ge, M. Ren, C. Sun, Z. Zhou, *J. Phys. Chem. C* **2009**, *114*, 251.
[28] Z.-M. Cui, L.-Y. Jiang, W.-G. Song, Y.-G. Guo, *Chem. Mater.* **2009**, *21*, 1162.
[29] Y. Chen, H. Xia, L. Lu, J. Xue, *J. Mater. Chem.* **2012**, *22*, 5006.
[30] W. M. Zhang, X. L. Wu, J. S. Hu, Y. G. Guo, L. J. Wan, *Adv. Funct. Mater.* **2008**, *18*, 3941.
[31] A. Débart, A. J. Paterson, J. Bao, P. G. Bruce, *Angew. Chem.* **2008**, *120*, 4597.
[32] F. Jiao, P. G. Bruce, *Adv. Mater.* **2007**, *19*, 657.
[33] S. Guo, H. Yu, P. Liu, X. Liu, C. Mingwei, M. Ishida, H. Zhou, *J. Mater. Chem. A* **2014**, *2*, 4422.
[34] T. Tao, A. M. Glushenkov, C. Zhang, H. Zhang, D. Zhou, Z. Guo, H. K. Liu, Q. Chen, H. Hu, Y. Chen, *J. Mater. Chem.* **2011**, *21*, 9350.
[35] Q. Wang , J. Xu, X. Wang, B. Liu, X. Hou, G. Yu, P. Wang, D. Chen, G. Shen, *ChemElectroChem* **2014**, *1*, 559.
[36] Y. Wang, T. Chen, *Electrochim. Acta* **2009**, *54*, 3510.
[37] X. Cao, Z. Yin, H. Zhang, *Energy Environ. Sci.* **2014**, *7*, 1850.
[38] F. Belliard, J. Irvine, *J. Power Sources* **2001**, *97*, 219.
[39] T. Yang, H. Zhang, Y. luo, L. Mei, D. Guo, Q. Li, T. Wang, *Electrochim. Acta* **2015**, *158*, 327.
[40] R. Singh, J. Singh, A. Singh, *Int. J. Hydrogen Energy* **2008**, *33*, 4260.
[41] J. Yao, Y. Gong, S. Yang, P. Xiao, Y. Zhang, K. Keyshar, G. Ye, S. Ozden, R. Vajtai, P. M. Ajayan, *ACS Appl. Mater. Interfaces* **2014**, *6*, 20414.
[42] S.-D. S. Kyung-Soo Park, H.-W. Shim, D.-W. Kim, *Nanoscale Res. Lett.* **2012**, *7*, 35.
[43] S. Han, D. Wu, S. Li, F. Zhang, X. Feng, *Small* **2013**, *9*, 1173.
[44] B. Luo, S. Liu, L. Zhi, *Small* **2012**, *8*, 630.

[45] N. Mahmood, C. Zhang, H. Yin, Y. Hou, *J. Mater. Chem. A* **2014**, *2*, 15.
[46] Z.-S. Wu, G. Zhou, L.-C. Yin, W. Ren, F. Li, H.-M. Cheng, *Nano Energy* **2012**, *1*, 107.
[47] Y. Zhao, X. F. Li, B. Yan, D. J. Li, S. Lawes, X. L. Sun, *J. Power Sources* **2015**, *274*, 869.
[48] G. S. R. Raju, E. Pavitra, Y. H. Ko, J. S. Yu, *J. Mater. Chem.* **2012**, *22*, 15562.
[49] J.-X. Cui, W.-S. Wang, L. Zhen, W.-Z. Shao, Z.-L. Chen, *CrystEngComm* **2012**, *14*, 7025.
[50] B. G. Xiangpeng Fang, Y. Shi, B. Li, C. Hua, C. Yao, Y. Zhang, Y.-S. Hu, Z. Wang, G. D. Stucky, L. Chen, *Nanoscale* **2012**, *4*, 1541.
[51] C. Yuan, H. B. Wu, Y. Xie, X. W. Lou, *Angew. Chem.* **2014**, *53*, 1488.
[52] Q. Song, Z. J. Zhang, *J. Am. Chem. Soc.* **2012**, *134*, 10182.
[53] P. Liu, Y. Huang, X. Sun, *Mater. Lett.* **2013**, *112*, 117.
[54] P. Liu, Y. Huang, X. Zhang, *Compos. Sci., Technol.* **2014**, *95*, 107.
[55] M. Zong, Y. Huang, H. Wu, Y. Zhao, Q. Wang, X. Sun, *Mater. Lett.* **2014**, *114*, 52.
[56] M. Fu, Q. Jiao, Y. Zhao, *J. Mater. Chem. A* **2013**, *1*, 5577.
[57] M. Zong, Y. Huang, N. Zhang, *Mater. Lett.* **2015**, *145*, 115.
[58] Z. Wang, X. Zhang, Y. Li, Z. Liu, Z. Hao, *J. Mater. Chem. A* **2013**, *1*, 6393.
[59] H. B. Wu, H. Pang, X. W. D. Lou, *Energy Environ. Sci.* **2013**, *6*, 3619.
[60] G. Zhang, X. W. D. Lou, *Sci. Rep.* **2013**, *3*, 1470.
[61] G. Zhang, X. W. D. Lou, *Adv. Mater.* **2013**, *25*, 976.
[62] B. Das, M. V. Reddy, S. Tripathy, B. V. R. Chowdari, *RSC Adv.* **2014**, *4*, 33883.
[63] F. Xia, X. Hu, Y. Sun, W. Luo, Y. Huang, *Nanoscale* **2012**, *4*, 4707.
[64] H. Yu, C. Guan, X. Rui, B. Ouyang, B. Yadian, Y. Huang, H. Zhang, H. E. Hoster, H. J. Fan, Q. Yan, *Nanoscale* **2014**, *6*, 10556.
[65] H. Wang, Y. Yang, Y. Liang, G. Zheng, Y. Li, Y. Cui, H. Dai, *Energy Environ. Sci.* **2012**, *5*, 7931.
[66] F. Cheng, J. Shen, B. Peng, Y. Pan, Z. Tao, J. Chen, *Nat. Chem.* **2011**, *3*, 79.
[67] G. Zhang, B. Y. Xia, X. Wang, X. W. D. Lou, *Adv. Mater.* **2014**, *26*, 2408.
[68] Y. Liang, H. Wang, J. Zhou, Y. Li, J. Wang, T. Regier, H. Dai, *J. Am. Chem. Soc.* **2012**, *134*, 3517.
[69] M. Zhang, M. Jia, Y. Jin, Q. Wen, C. Chen, *J. Alloys Compd* **2013**, *566*, 131.
[70] Y. Fu, Y. Wan, H. Xia, X. Wang, *J. Power Sources* **2012**, *213*, 338.
[71] C. T. Cherian, J. Sundaramurthy, M. V. Reddy, P. Suresh Kumar, K. Mani, D. Pliszka, C. H. Sow, S. Ramakrishna, B. V. Chowdari, *ACS Appl. Mater. Interfaces* **2013**, *5*, 9957.
[72] K. Xiao, L. Xia, G. Liu, S. Wang, L.-X. Ding, H. Wang, *J. Mater. Chem. A* **2015**, *3*, 6128.
[73] M.-C. Liu, L.-B. Kong, C. Lu, X.-M. Li, Y.-C. Luo, L. Kang, *Mater. Lett.* **2013**, *94*, 197.
[74] M. Inagaki, S. Nakai, T. Ikeda, *J. Nuclear Mater.* **1988**, *160*, 224.
[75] M. Asano, Y. Kato, T. Harada, Y. Mizutani, M. Yamawaki, *J. Nuclear Mater.* **1993**, *201*, 156.
[76] K. Moritani, H. Moriyama, *J. Nuclear Mater.* **1997**, *248*, 132.
[77] L. P. Teo, M. H. Buraidah, A. F. M. Nor, S. R. Majid, *Ionics* **2012**, *18*, 655.
[78] F. Belliard, J. Irvine, *Ionics* **2001**, *7*, 16.
[79] D. W. Zhang, S. Q. Zhang, Y. Jin, T. H. Yi, S. Xie, C. H. Chen, *J. Alloys, Compd.* **2006**, *415*, 229.
[80] L. P. Teo, M. H. Buraidah, N. A. Alias, M. Z. Kufian, S. R. Majid, A. K. Arof, *Mater. Res. Innovations* **2011**, *15*, s127.
[81] Q. Wang, Y. Huang, Y. Zhao, W. Zhang, Y. Wang, *Surf. Interface Anal.* **2013**, *45*, 1297.
[82] Y. Yao, Z. Yang, D. Zhang, W. Peng, H. Sun, S. Wang, *Ind. Eng. Chem. Res.* **2012**, *51*, 6044.
[83] Q. Wang, Y. Huang, J. Miao, Y. Wang, Y. Zhao, *Appl. Surf. Sci.* **2012**, *258*, 6923.
[84] Y. Zhao, Y. Huang, Q. Wang, W. Zhang, K. Wang, M. Zong, *J. Appl. ElectroChem.* **2013**, *43*, 1243.
[85] Q. Wang, Y. Huang, J. Miao, Y. Zhao, Y. Wang, *Mater. Lett* **2012**, *71*, 66.
[86] Q. Wang, Y. Huang, J. Miao, Y. Zhao, Y. Wang, *Appl. Surf. Sci.* **2012**, *258*, 9896.
[87] Y. Huang, Q. Wang, Y. Wang, *Micro Nano Lett.* **2012**, *7*, 1278.
[88] Y. Zhao, Y. Huang, Q. Wang, X. Wang, M. Zong, H. Wu, W. Zhang, *Electron. Mater. Lett.* **2013**, *9*, 683.
[89] Y. Zhao, Y. Huang, Q. Wang, X. Wang, M. Zong, *Ceramics Int.* **2013**, *39*, 1741.
[90] Y. Zhao, Y. Huang, Q. Wang, *Ceramics Int.* **2013**, *39*, 6861.
[91] R. Alcántara, G. F. Ortiz, P. Lavela, J. L. Tirado, *ElectroChem. Commun.* **2006**, *8*, 731.
[92] F. Huang, Z. Yuan, H. Zhan, Y. Zhou, J. Sun, *Mater. Lett.* **2003**, *57*, 3341.
[93] G. Wang, X. P. Gao, P. W. Shen, *J. Power Sources* **2009**, *192*, 719.
[94] S. Yuvaraj, S. Amaresh, Y. S. Lee, R. K. Selvan, *RSC Adv.* **2014**, *4*, 6407.
[95] Z. Wang, Z. Wang, W. Liu, W. Xiao, X. W. Lou, *Energy Environ. Sci.* **2013**, *6*, 87.
[96] J. Zhang, J. Liang, Y. Zhu, D. Wei, L. Fan, Y. Qian, *J. Mater. Chem. A* **2014**, *2*, 2728.
[97] Y. Cao, L. Zhang, D. Tao, D. Huo, K. Su, *Electrochim. Acta* **2014**, *132*, 483.
[98] P. Connor, J. Irvine, *J. Power Sources* **2001**, *97*, 223.
[99] Z. Wang, Z. Wang, H. Wu, X. W. Lou, *Sci. Rep.* **2013**, *3*, 1391.
[100] Z. Wang, L. Zhou, *Adv. Mater.* **2012**, *24*, 1903.
[101] X. W. D. Lou, L. A. Archer, Z. Yang, *Adv. Mater.* **2008**, *20*, 3987.
[102] Y. Qi, N. Du, H. Zhang, P. Wu, D. Yang, *J. Power Sources* **2011**, *196*, 10234.
[103] G. Fang, S. Kaneko, W. Liu, B. Xia, H. Sun, R. Zhang, J. Zheng, D. Li, *Appl. Surf. Sci.* **2013**, *283*, 963.
[104] Y. Zeng, T. Zhang, H. Fan, G. Lu, M. Kang, *Sens. Actuators B: Chem.* **2009**, *143*, 449.
[105] G. Ma, R. Zou, L. Jiang, Z. Zhang, Y. Xue, L. Yu, G. Song, W. Li, J. Hu, *CrystEngComm* **2012**, *14*, 2172.
[106] Z. Chen, M. Cao, C. Hu, *J. Phys. Chem. C* **2011**, *115*, 5522.
[107] X. Hu, T. Xiao, W. Huang, W. Tao, B. Heng, X. Chen, Y. Tang, *Appl. Surf. Sci.* **2012**, *258*, 6177.
[108] J. Huang, X. Xu, C. Gu, W. Wang, B. Geng, Y. Sun, J. Liu, *Sens. Actuators B: Chem.* **2012**, *171*, 572.
[109] Z. Li, Y. Zhou, C. Bao, G. Xue, J. Zhang, J. Liu, T. Yu, Z. Zou, *Nanoscale* **2012**, *4*, 3490.
[110] S. H. Choi, D. Hwang, D. Y. Kim, Y. Kervella, P. Maldivi, S. Y. Jang, R. Demadrille, I. D. Kim, *Adv. Funct. Mater.* **2013**, *23*, 3146.
[111] J. Chen, L. Lu, W. Wang, *J. Phys. Chem. C* **2012**, *116*, 10841.
[112] Y.-F. Wang, K.-N. Li, Y.-F. Xu, H.-S. Rao, C.-Y. Su, D.-B. Kuang, *Nanoscale* **2013**, *5*, 5940.
[113] E. L. Foletto, J. M. Simões, M. A. Mazutti, S. L. Jahn, E. I. Muller, L. S. F. Pereira, E. M. M. Flores, *Ceramics Int.* **2013**, *39*, 4569.
[114] L. Shi, Y. Dai, *J. Mater. Chem. A* **2013**, *1*, 12981.
[115] J. Zeng, M. Xin, K. Li, H. Wang, H. Yan, W. Zhang, *J. Phys. Chem. C* **2008**, *112*, 4159.
[116] X. J. Zhu, L. M. Geng, F. Q. Zhang, Y. X. Liu, L. B. Cheng, *J. Power Sources* **2009**, *189*, 828.
[117] J.-F. Duan, S.-C. Hou, S.-G. Chen, H.-G. Duan, *Mater. Lett.* **2014**, *122*, 261.
[118] N. Feng, S. Peng, X. Sun, L. Qiao, X. Li, P. Wang, D. Hu, D. He, *Mater. Lett.* **2012**, *76*, 66.
[119] S. M. Becker, M. Scheuermann, V. Sepelak, A. Eichhofer, D. Chen, R. Monig, A. S. Ulrich, H. Hahn, S. Indris, *Phys. Chem. Chem. Phys.* **2011**, *13*, 19624.
[120] F. Han, W. C. Li, C. Lei, B. He, K. Oshida, A. H. Lu, *Small* **2014**, *10*, 2637.

[121] C. T. Cherian, M. Zheng, M. V. Reddy, B. Chowdari, C. H. Sow, *ACS Appl. Mater. Interfaces* **2013**, *5*, 6054.
[122] Y. Chen, B. Qu, L. Mei, D. Lei, L. Chen, Q. Li, T. Wang, *J. Mater. Chem.* **2012**, *22*, 25373.
[123] Y. Zhao, Y. Huang, Q. Wang, K. Wang, M. Zong, L. Wang, W. Zhang, X. Sun, *RSC Adv.* **2013**, *3*, 14480.
[124] K. Wang, Y. Huang, H. Huang, Y. Zhao, X. Qin, X. Sun, Y. Wang, *Ceramics Int.* **2014**, *40*, 8021.
[125] C. T. Cherian, M. Zheng, M. V. Reddy, B. V. Chowdari, C. H. Sow, *ACS Appl. Mater. Interfaces* **2013**, *5*, 6054.
[126] A. Rong, X. Gao, G. Li, T. Yan, H. Zhu, J. Qu, D. Song, *J. Phys. Chem. B* **2006**, *110*, 14754.
[127] K. Kim, A. Annamalai, S. H. Park, T. H. Kwon, M. W. Pyeon, M.-J. Lee, *Electrochim. Acta* **2012**, *76*, 192.
[128] F. Han, W. C. Li, C. Lei, B. He, K. Oshida, A. H. Lu, *Small* **2014**, *10*, 2637.
[129] Y. Zhao, Y. Huang, Q. Wang, K. Wang, M. Zong, L. Wang, X. Sun, *Ceramics Int.* **2014**, *40*, 2275.
[130] W. Song, J. Xie, W. Hu, S. Liu, G. Cao, T. Zhu, X. Zhao, *J. Power Sources* **2013**, *229*, 6.
[131] Y. Zhao, Y. Huang, W. Zhang, Q. Wang, K. Wang, M. Zong, X. Sun, *RSC Adv.* **2013**, *3*, 23489.
[132] Q. Xie, Y. Ma, X. Zhang, H. Guo, A. Lu, L. Wang, G. Yue, D.-L. Peng, *Electrochim. Acta* **2014**, *141*, 374.
[133] Y. Sun, X. Hu, W. Luo, Y. Huang, *J. Mater. Chem.* **2012**, *22*, 425.
[134] Y. Zhao, Y. Huang, X. Sun, H. Huang, K. Wang, M. Zong, Q. Wang, *Electrochim. Acta* **2014**, *120*, 128.
[135] J. Liu, S. Tang, Y. Lu, G. Cai, S. Liang, W. Wang, X. Chen, *Energy Environ. Sci.* **2013**, *6*, 2691.
[136] L. Li, S. Peng, Y. L. Cheah, J. Wang, P. Teh, Y. Ko, C. Wong, M. Srinivasan, *Nanoscale* **2013**, *5*, 134.
[137] L. Li, S. Peng, J. Wang, Y. L. Cheah, P. Teh, Y. Ko, C. Wong, M. Srinivasan, *ACS Appl. Mater. Interfaces* **2012**, *4*, 6005.
[138] S. Zhao, Y. Bai, W.-F. Zhang, *Electrochim. Acta* **2010**, *55*, 3891.
[139] T. Xiao, Y. Tang, Z. Jia, S. Feng, *Electrochim. Acta* **2009**, *54*, 2396.
[140] S. Peng, L. Li, H. B. Wu, S. Madhavi, X. W. D. Lou, *Adv. Energy Mater.* **2015**, *5*, 1401172.
[141] Y. T. Xiaoyan Hu, T. Xiao, J. Jiang, Z. Jia, D. Li, B. Li, L. Luo, *J. Phys. Chem. C* **2010**, *114*, 947.
[142] Y. Li, S. Tan, J. Jiang, Z. Huang, X. Tan, *CrystEngComm* **2011**, *13*, 2649.
[143] M.-C. Liu, L.-B. Kong, X.-J. Ma, C. Lu, X.-M. Li, Y.-C. Luo, L. Kang, *New J. Chem.* **2012**, *36*, 1713.
[144] L. Q. Mai, F. Yang, Y. L. Zhao, X. Xu, L. Xu, Y. Z. Luo, *Nat. Commun.* **2011**, *2*, 381.
[145] C. Peng, L. Gao, S. Yang, J. Sun, *Chem. Commun.* **2008**, 5601.
[146] G. Kianpour, M. Salavati-Niasari, H. Emadi, *Superlattices, Microstructures* **2013**, *58*, 120.
[147] W. Xiao, J. S. Chen, C. M. Li, R. Xu, X. W. Lou, *Chem. Mater.* **2010**, *22*, 746.
[148] L. Robertson, M. Duttine, M. Gaudon, A. Demourgues, *Chem. Mater.* **2011**, *23*, 2419.
[149] C. Livage, A. Hynaux, J. Marrot, M. Nogues, G. Férey, *J. Mater. Chem.* **2002**, *12*, 1423.
[150] C. T. Cherian, M. V. Reddy, S. C. Haur, B. V. Chowdari, *ACS Appl. Mater. Interfaces* **2013**, *5*, 918.
[151] Y. Sharma, N. Sharma, G. V. Subba Rao, B. V. R. Chowdari, *Adv. Funct. Mater.* **2007**, *17*, 2855.
[152] J. Bai, X. Li, G. Liu, Y. Qian, S. Xiong, *Adv. Funct. Mater.* **2014**, *24*, 3012.
[153] M. V. Reddy, K. Y. H. Kenrick, T. Y. Wei, G. Y. Chong, G. H. Leong, B. V. R. Chowdari, *J. Electrochem. Soc.* **2011**, *158*, A1423.
[154] J. Li, S. Xiong, Y. Liu, Z. Ju, Y. Qian, *ACS Appl. Mater. Interfaces* **2013**, *5*, 981.
[155] G. Huang, S. Xu, Z. Xu, H. Sun, L. Li, *ACS Appl. Mater. Interfaces* **2014**, *6*, 21325.
[156] S. G. Mohamed, C. J. Chen, C. K. Chen, S. F. Hu, R. S. Liu, *ACS Appl. Mater. Interfaces* **2014**, *6*, 22701.
[157] N. Du, Y. Xu, H. Zhang, J. Yu, C. Zhai, D. Yang, *Inorg. Chem.* **2011**, *50*, 3320.
[158] W. Luo, X. Hu, Y. Sun, Y. Huang, *J. Mater. Chem.* **2012**, *22*, 8916.
[159] S. H. Choi, Y. C. Kang, *ChemSusChem* **2013**, *6*, 2111.
[160] J. Li, J. Wang, D. Wexler, D. Shi, J. Liang, H. Liu, S. Xiong, Y. Qian, *J. Mater. Chem. A* **2013**, *1*, 15292.
[161] Q. Xie, F. Li, H. Guo, L. Wang, Y. Chen, G. Yue, D. L. Peng, *ACS Appl. Mater. Interfaces* **2013**, *5*, 5508.
[162] G. Gao, H. B. Wu, S. Ding, X. W. Lou, *Small* **2015**, *11*, 432.
[163] J. Zhu, Z. Xu, B. Lu, *Nano Energy* **2014**, *7*, 114.
[164] Q. Zhang, H. Chen, J. Wang, D. Xu, X. Li, Y. Yang, K. Zhang, *ChemSusChem* **2014**, *7*, 2325.
[165] X. Y. Yu, X. Z. Yao, T. Luo, Y. Jia, J. H. Liu, X. J. Huang, *ACS Appl. Mater. Interfaces* **2014**, *6*, 3689.
[166] L. Li, Y. Cheah, Y. Ko, P. Teh, G. Wee, C. Wong, S. Peng, M. Srinivasan, *J. Mater. Chem. A* **2013**, *1*, 10935.
[167] J. Liu, C. Liu, Y. Wan, W. Liu, Z. Ma, S. Ji, J. Wang, Y. Zhou, P. Hodgson, Y. Li, *CrystEngComm* **2013**, *15*, 1578.
[168] Y. Chen, M. Zhuo, J. Deng, Z. Xu, Q. Li, T. Wang, *J. Mater. Chem. A* **2014**, *2*, 4449.
[169] H. S. Jadhav, R. S. Kalubarme, C. N. Park, J. Kim, C. J. Park, *Nanoscale* **2014**, *6*, 10071.
[170] A. K. Mondal, D. Su, S. Chen, X. Xie, G. Wang, *ACS Appl. Mater. Interfaces* **2014**, *6*, 14827.
[171] L. Shen, Q. Che, H. Li, X. Zhang, *Adv. Funct. Mater.* **2014**, *24*, 2630.
[172] L. Wang, L. Zhuo, C. Zhang, F. Zhao, *ACS Appl. Mater. Interfaces* **2014**, *6*, 10813.
[173] X. Yao, C. Zhao, J. Kong, D. Zhou, X. Lu, *RSC Adv.* **2014**, *4*, 37928.
[174] H. Liu, J. Wang, *J. Electron. Mater.* **2012**, *41*, 3107.
[175] B. Liu, J. Zhang, X. Wang, G. Chen, D. Chen, C. Zhou, G. Shen, *Nano Lett.* **2012**, *12*, 3005.
[176] B. Liu, X. Wang, B. Liu, Q. Wang, D. Tan, W. Song, X. Hou, D. Chen, G. Shen, *Nano Res.* **2013**, *6*, 525.
[177] S. G. Mohamed, T.-F. Hung, C.-J. Chen, C. K. Chen, S.-F. Hu, R.-S. Liu, K.-C. Wang, X.-K. Xing, H.-M. Liu, A.-S. Liu, M.-H. Hsieh, B.-J. Lee, *RSC Adv.* **2013**, *3*, 20143.
[178] H. Long, T. Shi, S. Jiang, S. Xi, R. Chen, S. Liu, G. Liao, Z. Tang, *J. Mater. Chem. A* **2014**, *2*, 3741.
[179] B. Qu, L. Hu, Q. Li, Y. Wang, L. Chen, T. Wang, *ACS Appl. Mater. Interfaces* **2014**, *6*, 731.
[180] Z. P. Sun, W. Ai, J. Liu, X. Qi, Y. Wang, J. Zhu, H. Zhang, T. Yu, *Nanoscale* **2014**, *6*, 6563.
[181] G. Gao, H. B. Wu, B. Dong, S. Ding, X. W. D. Lou, *Adv. Sci.* **2015**, *2*, 140014.
[182] G. Gao, H. B. Wu, X. W. D. Lou, *Adv. Energy Mater.* **2014**, *4*, 1400422.
[183] X. Q. Renbing Wu, K. Zhou, J. Wei, J. Lou, P. M. Ajayan, *ACS Nano* **2014**, *8*, 6297.
[184] L. Song, J. Zhang, L. Sun, F. Xu, F. Li, H. Zhang, X. Si, C. Jiao, Z. Li, S. Liu, Y. Liu, H. Zhou, D. Sun, Y. Du, Z. Cao, Z. Gabelica, *Energy Environ. Sci.* **2012**, *5*, 7508.
[185] B. Liu, X. Zhang, H. Shioyama, T. Mukai, T. Sakai, Q. Xu, *J. Power Sources* **2010**, *195*, 857.
[186] X. Xu, R. Cao, S. Jeong, J. Cho, *Nano Lett.* **2012**, *12*, 4988.
[187] A. Banerjee, U. Singh, V. Aravindan, M. Srinivasan, S. Ogale, *Nano Energy* **2013**, *2*, 1158.
[188] Y. Han, P. Qi, S. Li, X. Feng, J. Zhou, H. Li, S. Su, X. Li, B. Wang, *Chem. Commun* **2014**, *50*, 8057.

[189] D. Bresser, E. Paillard, R. Kloepsch, S. Krueger, M. Fiedler, R. Schmitz, D. Baither, M. Winter, S. Passerini, *Adv. Energy Mater.* **2013**, *3*, 513.
[190] F. Martinez-Julian, A. Guerrero, M. Haro, J. Bisquert, D. Bresser, E. Paillard, S. Passerini, G. Garcia-Belmonte, *J. Phys. Chem. C* **2014**, *118*, 6069.
[191] Z. Xing, Z. Ju, J. Yang, H. Xu, Y. Qian, *Nano Res.* **2012**, *5*, 477.
[192] J. M. Won, S. H. Choi, Y. J. Hong, Y. N. Ko, Y. C. Kang, *Sci. Rep.* **2014**, *4*, 5857.
[193] L. Luo, R. Cui, K. Liu, H. Qiao, Q. Wei, *Ionics* **2014**, *21*, 687.
[194] X. Yao, J. Kong, X. Tang, D. Zhou, C. Zhao, R. Zhou, X. Lu, *RSC Adv.* **2014**, *4*, 27488.
[195] P. F. Teh, Y. Sharma, S. S. Pramana, M. Srinivasan, *J. Mater. Chem.* **2011**, *21*, 14999.
[196] J. G. Kim, Y. Kim, Y. Noh, W. B. Kim, *RSC Adv.* **2014**, *4*, 27714.
[197] Y. Deng, Q. Zhang, S. Tang, L. Zhang, S. Deng, Z. Shi, G. Chen, *Chem. Commun* **2011**, *47*, 6828.
[198] L. Yao, X. Hou, S. Hu, Q. Ru, X. Tang, L. Zhao, D. Sun, *J. Solid State ElectroChem.* **2013**, *17*, 2055.
[199] Y. Wang, D. Su, A. Ung, J. H. Ahn, G. Wang, *Nanotechnology* **2012**, *23*, 055402.
[200] L. Hou, L. Lian, L. Zhang, G. Pang, C. Yuan, X. Zhang, *Adv. Funct. Mater.* **2015**, *25*, 238.
[201] Z. H. Li, T. P. Zhao, X. Y. Zhan, D. S. Gao, Q. Z. Xiao, G. T. Lei, *Electrochim. Acta* **2010**, *55*, 4594.
[202] L. Wu, Q. Xiao, Z. Li, G. Lei, P. Zhang, L. Wang, *Solid State Ionics* **2012**, *215*, 24.
[203] J. Sui, C. Zhang, D. Hong, J. Li, Q. Cheng, Z. Li, W. Cai, *J. Mater. Chem.* **2012**, *22*, 13674.
[204] H. Xia, Y. Qian, Y. Fu, X. Wang, *Solid State Sci.* **2013**, *17*, 67.
[205] B. Wang, S. Li, B. Li, J. Liu, M. Yu, *New J. Chem.* **2015**, *39*, 1725.
[206] P. R. Kumar, P. Kollu, C. Santhosh, K. Eswara Varaprasada Rao, D. K. Kim, A. N. Grace, *New J. Chem.* **2014**, *38*, 3654.
[207] C. Zhao, C. Yu, S. Liu, J. Yang, X. Fan, J. Qiu, *Particle Particle Systems Charact.* **2015**, *32*, 91.
[208] S. Li, B. Wang, J. Liu, M. Yu, *Electrochim. Acta* **2014**, *129*, 33.
[209] L. Lin, Q. Pan, *J. Mater. Chem. A* **2015**, *3*, 1724.
[210] G. Huang, F. Zhang, L. Zhang, X. Du, J. Wang, L. Wang, *J. Mater. Chem. A* **2014**, *2*, 8048.
[211] F. Zou, X. Hu, Z. Li, L. Qie, C. Hu, R. Zeng, Y. Jiang, Y. Huang, *Adv. Mater.* **2014**, *26*, 6622.
[212] Y. Yang, Y. Zhao, L. Xiao, L. Zhang, *Electrochem. Commun.* **2008**, *10*, 1117.
[213] L. Xiao, Y. Yang, J. Yin, Q. Li, L. Zhang, *J. Power Sources* **2009**, *194*, 1089.
[214] Y. Deng, S. Tang, Q. Zhang, Z. Shi, L. Zhang, S. Zhan, G. Chen, *J. Mater. Chem.* **2011**, *21*, 11987.
[215] S.-W. Kim, H.-W. Lee, P. Muralidharan, D.-H. Seo, W.-S. Yoon, D. K. Kim, K. Kang, *Nano Res.* **2011**, *4*, 505.
[216] X.-F. Chen, L. Qie, L.-L. Zhang, W.-X. Zhang, Y.-H. Huang, *J. Alloys, Compounds* **2013**, *559*, 5.
[217] M. H. Kim, Y. J. Hong, Y. C. Kang, *RSC Adv.* **2013**, *3*, 13110.
[218] C. Yuan, J. Li, L. Hou, L. Zhang, X. Zhang, *Particle Particle Systems Charact.* **2014**, *31*, 657.
[219] L. Yu, L. Zhang, H. B. Wu, G. Zhang, X. W. Lou, *Energy Environ. Sci.* **2013**, *6*, 2664.
[220] L. Zhou, H. B. Wu, T. Zhu, X. W. Lou, *J. Mater. Chem.* **2012**, *22*, 827.
[221] G. Zhang, L. Yu, H. B. Wu, H. E. Hoster, X. W. Lou, *Adv. Mater.* **2012**, *24*, 4609.
[222] L. Zhou, D. Zhao, X. W. Lou, *Adv. Mater.* **2012**, *24*, 745.
[223] L. Hu, H. Zhong, X. Zheng, Y. Huang, P. Zhang, Q. Chen, *Sci. Rep.* **2012**, *2*, 986.
[224] J. Haetge, I. Djerdj, T. Brezesinski, *Chem. Commun.* **2012**, *48*, 6726.
[225] D. P. Dubal, P.G- Romero, B. R. Sankapal, R. Holze, *Nano Energy* **2015**, *11*, 377.
[226] D. Chen, Q. F. Wang, R. M. Wang, G. Z. Shen, *J. Mater. Chem. A* **2015**, *3*, 10158.
[227] C. Wu, J. Maier, Y. Yu, *Adv. Funct. Mater.* **2015**, *25*, 3488.
[228] Y. Ma, Q. Xie, X. Liu, Y. Zhao, D. Zeng, L. Wang, Y. Zheng, D.-L. Peng, *Electrochim. Acta* **2015**, *182*, 327.
[229] S. Yuvaraj, W. J. Lee, C. W. Lee, R. K. Selvan, *RSC Adv.* **2015**, *5*, 67210.
[230] Y.-L. Qin, F.-F. Zhang, X.-C. Du, G. Huang, Y.-C. Liu, L.-M. Wang, *J. Mater. Chem. A* **2015**, *3*, 2985.
[231] X. Chen, Y. Huang, H. Huang, M. Wang, K. Wang, *Mater. Lett.* **2015**, *149*, 33.
[232] J. H. Ahn, G. D. Park, Y. C. Kang, J.-H. Lee, *Electrochim. Acta* **2015**, *174*, 102.
[233] Y. Wang, J. Ke, Y. Zhang, Y. Huang, *J. Mater. Chem. A* **2015**, *3*, 24303.
[234] X.-B. Zhong, H.-Y. Wang, Z.-Z. Yang, B. Jin, Q.-C. Jiang, *J. Power Sources* **2015**, *296*, 298.
[235] L. Guo, Q. Ru, X. Song, S. Hu, Y. Mo, *J. Mater. Chem. A* **2015**, *3*, 8683.
[236] L. Guo, Q. Ru, X. Song, S. Hu, Y. Mo, *RSC Adv.* **2015**, *5*, 19241.
[237] a) A. K. Mondal, D. Su, S. Chen, K. Kretschmer, X. Xie, H. J. Ahn, G. Wang, *ChemPhysChem.* **2015**, *16*, 169; b) T. Li, X. Li, Z. Wang, H. Guo, Y. Li, *J. Mater. Chem. A* **2015**, *3*, 11970.
[238] A. K. Mondal, D. Su, S. Chen, A. Ung, H. S. Kim, G. Wang, *Chemistry* **2015**, *21*, 1526.
[239] S. Liu, J. Wu, J. Zhou, G. Fang, S. Liang, *Electrochim. Acta* **2015**, *176*, 1.
[240] J. Cheng, Y. Lu, K. Qiu, H. Yan, J. Xu, L. Han, X. Liu, J. Luo, J. K. Kim, Y. Luo, *Sci. Rep.* **2015**, *5*, 12099.
[241] X. Ge, Z. Li, C. Wang, L. Yin, *ACS Appl. Mater. Interfaces* **2015**, *7*, 26633.
[242] Z. Li, L. Yin, *J. Mater. Chem. A* **2015**, *3*, 21569.
[243] Z. Zhang, Y. Ji, J. Li, Q. Tan, Z. Zhong, F. Su, *ACS Appl. Mater. Interfaces* **2015**, *7*, 6300.
[244] H. Yue, Q. Wang, Z. Shi, C. Ma, Y. Ding, N. Huo, J. Zhang, S. Yang, *Electrochim. Acta* **2015**, *180*, 622.
[245] K. Wang, Y. Huang, D. Wang, Y. Zhao, M. Wang, X. Chen, X. Qin, S. Li, *RSC Adv.* **2015**, *5*, 107247.
[246] H. Yu, H. Fan, B. Yadian, H. Tan, W. Liu, H. H. Hng, Y. Huang, Q. Yan, *ACS Appl. Mater. Interfaces* **2015**, *7*, 26751.
[247] W. Kang, Y. Tang, W. Li, X. Yang, H. Xue, Q. Yang, C. S. Lee, *Nanoscale* **2015**, *7*, 225.
[248] P. Li, J. Liu, Y. Liu, Y. Wang, Z. Li, W. Wu, Y. Wang, L. Yin, H. Xie, M. Wu, X. He, J. Qiu, *Electrochim. Acta* **2015**, *180*, 164.
[249] Y. Zhang, Y. Zhang, C. Guo, B. Tang, X. Wang, Z. Bai, *Electrochim. Acta* **2015**, *182*, 1140.
[250] L. Zhang, S. Zhu, H. Cao, L. Hou, C. Yuan, *Chemistry* **2015**, *21*, 10771.
[251] X. Meng, X. Yang, X. Sun, *Adv. Mater.* **2012**, *24*, 3589.
[252] J. Liu, X. Sun, *Nanotechnol.* **2015**, *26*, 024001.
[253] R. Zou, Z. Zhang, M. Yuen, M. Sun, J. Hu, C. Lee ,W. Zhang, *NPG Asia Mater.* **2015**, *7*, 195.
[254] Y. Zhao, Z. Song, X. Li, Q. Sun, N. Cheng, S. Lawes, X. Sun, *Energy Storage Mater.* **2016**, *2*, 35.